The Journal of Immunology
RESEARCH ARTICLE | MARCH 24 2023

CARD19, a Novel Regulator of the TAK1/NF-κB Pathway in Self-Reactive B Cells

Yongwei Zheng; ... et. al

J Immunol (2023) 210 (9): 1222–1235.
https://doi.org/10.4049/jimmunol.2200639

CARD19, a Novel Regulator of the TAK1/NF-κB Pathway in Self-Reactive B Cells

Yongwei Zheng,* Mei Yu,* Yuhong Chen,* Liquan Xue,† Wen Zhu,*,‡ Guoping Fu,* Stephan W. Morris,† Renren Wen,*,‡ and Demin Wang*,‡

The caspase recruitment domain family member (CARD)11-Bcl10-Malt1 signalosome controls TGF-β–activated kinase 1 (TAK1) activation and regulates BCR-induced NF-κB activation. In this study, we discovered that CARD19 interacted with TAK1 and inhibited TAB2-mediated TAK1 ubiquitination and activation. Although CARD19 deficiency in mice did not affect B cell development, it enhanced clonal deletion, receptor editing, and anergy of self-reactive B cells, and it reduced autoantibody production. Mechanistically, CARD19 deficiency increased BCR/TAK1-mediated NF-κB activation, leading to increased expression of transcription factors Egr2/3, as well as the E3 ubiquitin ligases c-Cbl/Cbl-b, which are known inducers of B cell tolerance in self-reactive B cells. RNA sequencing analysis revealed that although CARD19 deficiency did not affect the overall Ag-induced gene expression in naive B cells, it suppressed BCR signaling and increased hyporesponsiveness of self-reactive B cells. As a result, CARD19 deficiency prevented Bm12-induced experimental systemic lupus erythematosus. In summary, CARD19 negatively regulates BCR/TAK1-induced NF-κB activation and its deficiency increases Egr2/3 and c-Cbl/Cbl-b expression in self-reactive B cells, thereby enhancing B cell tolerance. ***The Journal of Immunology*****, 2023, 210: 1222–1235.**

B cells go through several stages of development, including pro, pre, immature, and mature stages (1, 2). At the immature stage, B cells develop a functional BCR) made up of Ig H and L chains and then differentiate into mature B cells (1–3). Immature B cells with a self-reactive BCR may be negatively selected through one of three mechanisms: clonal deletion, receptor editing, and anergy (1). The BCR signaling threshold controls the process of negative selection. Highly self-reactive cells initiate new L chain rearrangement to change the specificity of the BCR through receptor editing or undergo clonal deletion through apoptosis (4–7). Weak self-reactive cells, in contrast, may escape to the periphery and become unresponsive to Ags, a state known as anergy (8, 9). Up to half of all newly generated B cells are anergic, a key mechanism of immune tolerance (10). Anergy is a reversible process and is maintained through constant stimulation by self-antigens and is characterized by suppressed BCR signaling (11, 12). However, it is not fully understood how this suppression occurs. Disruption in negative regulators of BCR signaling, such as Lyn, SHP-1, SHIP-1, CD22, and c-Cbl/Cbl-b, can lead to elevated BCR signaling and the breakdown of B cell tolerance (13–17).

The BCR activates three protein tyrosine kinases (LYN, SYK, and BTK) through transmembrane molecules Igα and Igβ. This leads to the activation of several signaling pathways that regulate the proliferation, survival, and effector functions of B cells (18–21). The NF-κB pathway plays a crucial role in these biological processes and is tightly regulated in B cells (22). Genetic deletions of the signaling components of the NF-κB pathway can cause immune deficiencies (23), and persistent, abnormal activation of NF-κB is associated with autoimmune disorders (24). Caspase recruitment domain-containing membrane-associated guanylate kinase protein-1 (CARMA1 or caspase recruitment domain family member [CARD]11), B cell lymphoma 10 (BCL10), and MALT lymphoma translocation protein 1 (MALT1) forms the CARMA1/CARD11-BCL10-MALT1 (CBM) signalosome complex that is central to BCR-induced NF-κB activation (25, 26). Deletions of individual component of the CBM complex impair BCR-induced NF-κB activation, B cell maturation, and immune responses, highlighting the vital role of the intact CBM complex in activating the BCR-induced NF-κB pathway and B cell biology (27–31). The CBM complex activates the TGF-β–activated kinase 1 (TAK1) (32). TAK1 activation involves its association with

*Versiti Blood Research Institute, Milwaukee, WI; †HealthChart LLC, Memphis, TN; and ‡Department of Microbiology and Immunology, Medical College of Wisconsin, Milwaukee, WI

ORCIDs: 0000-0002-1947-5386 (Y.Z.); 0000-0002-7734-9943 (W.Z.); 0000-0003-2420-8212 (R.W.).

Received for publication August 29, 2022. Accepted for publication February 22, 2023.

This work was supported in part by the Division of Microbiology and Infectious Diseases, National Institute of Allergy and Infectious Diseases Grant AI079087 (to D.W.) and by NHLBI Division of Intramural Research Grants HL130724 (to D.W.), HL148120 (to R.W.), and HL161127 (to R.W.). Y.Z. is supported by an Elizabeth Elser Doolittle Trust postdoctoral fellowship. W.Z. is supported by an American Heart Association predoctoral fellowship.

Y.Z. contributed to experimental design, performed the experiments, analyzed the results, and wrote the draft of the manuscript; M.Y., Y.C., W.Z., and G.F. performed some experiments; L.X. generated CARD19-deficient mice and the anti-CARD19 Ab at St. Jude Children's Research Hospital; S.W.M. generated CARD19-deficient mice and the anti-CARD19 Ab at St. Jude Children's Research Hospital and critically read the manuscript; R.W. provided intellectual input, supervised the study, and critically reviewed the manuscript; and D.W. conceived and supervised the study, analyzed the results, and wrote the manuscript.

Address correspondence and reprint requests to Dr. Renren Wen and Dr. Demin Wang, Versiti Blood Research Institute, 8727 West Watertown Plank Road, Milwaukee, WI 53226. E-mail addresses: rwen@versiti.org (R.W.) and dwang@versiti.org (D.W.)

The online version of this article contains supplemental material.

Abbreviations used in this article: ANA, antinuclear Ab; BCL10, B cell lymphoma 10; BinCARD, BCL10-interacting protein with CARD; BM, bone marrow; CARD, caspase recruitment domain family member; CARMA1, caspase recruitment domain-containing membrane-associated guanylate kinase protein-1; CBM, CARMA1/CARD11-BCL10-MALT1; co-IP, coimmunoprecipitation; Egr, early growth response; ES cell, embryonic stem cell; GC, germinal center; GSEA, gene set enrichment analysis; Ig^{HEL} mice, MD4 mice that express a transgene encoding Ig specific for hen egg lysozyme; IKK, IκB kinase; IP, immunoprecipitation; MALT1, MALT lymphoma translocation protein 1; PCA, principal component analysis; PDBu, phorbol 12, 13-dibutyrate; PLC, phospholipase C; RNA-seq, RNA sequencing; sHEL mice, ML5 mice that express the soluble form of the cognate Ag HEL; SLE, systemic lupus erythematosus; TAK1, TGF-β–activated kinase 1; TRAF6, TNFR-associated factor 6;

the regulatory proteins TAB1 and TAB2 (33–35). TAB2 recruits the ubiquitin ligase TNFR-associated factor 6 (TRAF6), which mediates the ubiquitination of BCL10 and TAK1, leading to TAK1 activation and the subsequent recruitment of the IκB kinase (IKK) complex through NEMO, the ubiquitin-binding subunit of IKK (36). In turn, TAK1 activates IKK, which phosphorylates IκB, triggering IκB degradation and the subsequent nuclear localization of NF-κB (37, 38).

CARD19 is a protein that belongs to the death domain superfamily, which includes the death domain subfamily, death effector domain subfamily, CARD domain subfamily, and pyrin domain subfamily. Many members of this family are important for regulating the immune response (39). Human CARD19 is originally identified from the expressed sequence tag (EST) database as BCL10-interacting protein with CARD (BinCARD)1 that contains 228 aa (40). BinCARD1 has been shown to interact with BCL10 and to suppress BCL10-mediated activation of NF-κB, and it reduces TCR-induced BCL10 phosphorylation in Jurkat T cells when it is overexpressed (40). Recent studies have found that BinCARD1 is an incompletely derived *C9orf89* gene product whereas BinCARD2 with 183 aa is the properly spliced and the most abundant isoform (41). Overexpression of BinCARD2 inhibits BCL10-induced NF-κB activation in HEK293T cells, and knockdown of BinCARD2 leads to dysregulation of the IFN response in cell lines (41, 42). However, the in vivo biological function of BinCARD2, also known as CARD19, is currently unknown.

In this study, we identified that CARD19 strongly interacted with TAK1, but not the other components of the CBM signalosome, and was able to inhibit TAB2-mediated TAK1 activation and subsequent NF-κB activation. We found that CARD19 deficiency did not have an impact on B cell development or the gene expression and humoral immune response induced by foreign Ags. However, CARD19 deficiency was observed to enhance self-antigen–induced tolerance and prevent autoimmunity through the induction of ERG2/3 and c-Cbl/Cbl-b in autoreactive B cells by modulating the NF-κB pathway.

Materials and Methods

Mice

MD4 mice that express a transgene encoding Ig specific for hen egg lysozyme (Ig^{HEL} mice; IghelMD4, stock no. 002595) mice, ML5 mice that express the soluble form of the cognate Ag HEL (sHEL; ML5sHEL, stock no. 002599) transgenic mice, Bm12 (stock no. 001162) mice, and μMT (stock no. 002288) mice were purchased from The Jackson Laboratory. CD45.1 congenic (stock no. 564) mice were purchased from Charles River Laboratories. c-Rel–deficient mice were provided by Dr. Shigeki Miyamoto at the University of Wisconsin–Madison. Experimental and control mice were 8–10 wk old. Mice were maintained at the Biological Resource Center at the Medical College of Wisconsin. All animal protocols were approved by the Medical College of Wisconsin Institutional Animal Care and Use Committee.

Generation of CARD19-deficient mice

A *Card19* targeting vector was constructed by using an XbaI/Not I fragment of the *Card19* genomic DNA locus. The fragment included exon 2 to exon 6 of the *Card19* gene and its flanking sequences, which were replaced by a neo expression cassette. The 3′ end of the *Card19-neo* construct also contains a HSV-thymidine kinase (TK) gene cassette that provides for negative selection of the embryonic stem cells (ES cells) via ganciclovir. The targeting construct was linearized and electroporated into E14 ES cells as described (43). The correctly targeted ES cell clones with normal karyotypes were selected by normal karyotypes and then injected into blastocysts to generate chimeric mice. These mice were then bred to obtain germline transmission.

The genotypes of the mice were determined by PCR using specific primers. The expression of Card19 in tissues from wild-type and CARD19-deficient mice was assessed by quantitative real-time PCR or immunoblot using a CARD19-specific polyclonal Ab. Finally, CARD19-deficient mice were backcrossed to a C57BL/6 genetic background. A high-throughput genome scan revealed that the Card19-mutant colony had a 90:10 C57BL/6J and 129 background.

Abs used

The cells were stained with a combination of fluorescence-conjugated Abs specific for different cell surface markers. The following Abs were used for staining: allophycocyanin-conjugated anti-B220, anti-IgM, anti–c-Kit, and anti-F4/80; PE-conjugated anti-CD4, anti-CD86, anti-FcεR, anti-CD11b, anti-Gr1, and anti-Ter119; PE-Cy7–conjugated anti-B220, anti-CD8, anti-NK1.1, and anti-CD23; and biotin-conjugated anti-CD11c were purchased from eBioscience; allophycocyanin-conjugated anti-Thy1.2, anti-CD5 and streptavidin, and PE-conjugated anti-CD86 and anti-CD21 were purchased from BD Biosciences; PE-conjugated anti-IgD and FITC-conjugated anti-mouse λ L chain were purchased from SouthernBiotech; and allophycocyanin-Cy7–conjugated anti-B220 and anti-Ly6G were purchased from BioLegend.

Immunoblotting used the following various Abs. Rabbit anti-CARD19 polyclonal Ab that targeted the N-terminal 100 aa of mouse CARD19 was generated at St. Jude Children's Research Hospital. Anti-ERK1/2 (sc-093), anti–phospho-ERK1/2 ($pThr^{202}/pTyr^{204}$, sc-7383), anti-Akt (sc-8312), anti-JNK (sc-571), anti-p38 (sc-535), anti–phospholipase C (PLC)γ2 (sc-407), anti–Cbl-b (sc-8006), anti–c-Cbl (sc-1651), and anti-SHP1 (sc-287) Abs were purchased from Santa Cruz Biotechnology. Anti–phospho-Akt ($pThr^{308}$, no. 9275), anti–phospho-JNK ($pThr^{183}/pTyr^{185}$, no. 4668), anti–phospho-p38 ($pThr^{180}/pTyr^{182}$, no. 9216), anti–phospho-IκBα ($pSer^{32}/pSer^{36}$, no. 9246), anti-IκBα (no. 9242), anti–early growth response (Egr)3 (no. 2559), and anti–c-Rel (no. 12707) Abs were purchased from Cell Signaling Technology. Anti-Egr2 (PA5-27814) Ab was purchased from Invitrogen. Anti-NFATc1 (ALX-804-022-R100) Ab was purchased from Enzo Life Sciences. Anti-actin (MAB1501R) Ab was purchased from Millipore.

Immunoprecipitation (IP) used the following Abs: anti-MYC (sc-40, Santa Cruz Biotechnology), anti-FLAG (F3165, Sigma Aldrich), or anti-hemagglutinin (H9658, Sigma Aldrich) Abs. To check the ubiquitination of TAK1, anti-ubiquitin (sc-8017) Ab from Santa Cruz Biotechnology was used.

Bone marrow transplantation

To generate bone marrow (BM) chimeric mice, BM cells from wild-type or CARD19-deficient mice were mixed with BM cells from μMT mice at a 1:4 ratio and then transplanted into lethally irradiated (1000 rad) μMT mice via i.v. injection (5×10^6 cells/recipient). Eight weeks after transplantation, the recipient mice were used for the studies.

To generate BM transplanted mice for the Bm12-induced systemic lupus erythematosus (SLE) mouse model, BM cells from wild-type or CARD19-deficient mice were transplanted into lethally irradiated (1000 rad) B6.SJL-CD45.1 mice by i.v. injection (5×10^6 cells/recipient). Eight weeks after transplantation, the recipient mice were used for Bm12-induced SLE experiments.

Quantification of basal serum Igs

Serum Ig levels were quantified using an ELISA. The procedure involved coating Immuno 96-well plates with goat anti-mouse Ig (H+L) (Southern-Biotech) at a concentration of 2 μg/ml in PBS. Plates were then washed three times with 200 μl of 0.1% Tween 20 in PBS, followed by an incubation of 1 h with 1% BSA in PBS. Diluted serum samples and standards were then added into the ELISA plates and incubated for 1 h. For the measurement of IgM, the serum samples were diluted 1:10,000 with 1% BSA/PBS; for the measurement of IgG1 level, serum samples were diluted 1:20,000; and for measurement of IgG2c, IgG2b, and IgG3 levels, the serum samples were diluted 1:5,000. Unbound Abs were removed by washing the plates under the same conditions, before incubating them with HRP-conjugated secondary Abs for 1 h. The plates were then washed again, and tetramethylbenzidine substrates were added. The reactions were terminated by adding 1 N sulfuric acid, and ODs were measured at 450 nm.

T cell–dependent and T cell–independent Ag immunizations

T cell–dependent and T cell–independent Ag immunizations were performed as described previously (44). Briefly, 8- to 10-wk-old mice were immunized i.p. with 100 μg of the T cell–dependent Ag nitrophenyl–keyhole limpet hemocyanin (supplied by Biosearch Technologies) mixed 1:1 with Alum adjuvant (Pierce) (200 μl/mouse) or 50 μg of the T cell–independent Ag trinitrophenyl-Ficoll (supplied by Biosearch Technologies) mixed 1:1 with Alum adjuvant (200 μl/mouse). Sera were collected before and at various time points following the immunization. The levels of Ag-specific Abs in the serum were measured using ELISA.

Autoantibody profiling with autoantigen microarray

Autoantibodies against a panel of 124 autoantigens were measured using an autoantigen microarray platform developed by The University of Texas Southwestern Medical Center (https://microarray.swmed.edu/products/category/protein-array/). Serum samples were pretreated with DNase I and then diluted 1:50 in PBS with Tween 20 buffer for autoantibody profiling. The autoantigen array, which includes 124 autoantigens and four control proteins, was printed in duplicates onto nitrocellulose film slides (Grace Bio-Labs). The diluted serum samples were then incubated with the arrays, and autoantibodies were detected with Cy3-labeled anti-mouse IgG and Cy5-labeled anti-mouse IgM using a GenePix 4200A scanner (Molecular Devices) with a laser wavelength of 532 and 635 nm. The resulting images were analyzed using GenePix Pro 6.0 software (Molecular Devices). The median signal intensity for each spot was calculated and subtracted from the local background around the spot. Data from duplicate spots were then averaged. The background-subtracted signal intensity of each Ag was normalized to the average intensity of total mouse IgG or IgM, which was included on the array as an internal control. Finally, the net fluorescence intensity for each Ag was calculated by subtracting a PBS control, which was included for each experiment as a negative control. The signal-to-noise ratio was used as a quantitative measurement of the true signal above background noise. Signal-to-noise ratio values ≥ 3 were considered significantly higher than background and therefore true signals. The net fluorescence intensity of each autoantibody was used to generate heatmaps using the Morpheus platform (https://software.broadinstitute.org/morpheus/).

In vitro kinase assay

FLAG-tagged TAK1 protein was immunoprecipitated from HEK293T cells using an anti-FLAG Ab and the IP was carried out at 4°C for 3 h. The immunoprecipitates were then washed four times with lysis buffer (20 mM Tris [pH 7.0], 250 mM NaCl, 3 mM EDTA, 3 mM EGTA, 0.5% Nonidet P-40, 2 mM DTT, 0.5 mM PMSF, 20 mM β-glycerol phosphate, 1 mM Na_3VO_4, 1 μg/ml leupeptin, 1 μg/ml aprotinin, 10 mM p-nitrophenyl phosphate, 1 mM NaF), and twice with kinase buffer containing 50 mM Tris (pH 7.5), 5 mM $MgCl_2$, 1 mM DTT, 0.5 mM PMSF, 10 mM β-glycerol phosphate, 300 μM Na_3VO_4, 10 mM NaF, 1 μg/ml leupeptin, 1 μg/ml aprotinin, 10 mM *p*-nitrophenyl phosphate, and 10 μM ATP. Bacterially expressed and purified GST-IKKβ (1 μg) was used as the substrate. The immunoprecipitated FLAG-TAK1 was then incubated with the substrates in the kinase buffer with 0.1 μCi of ^{32}P-γ-ATP (NEG002Z250, PerkinElmer) at 30°C for 1 h. After the reactions, the samples were stopped by adding 2× SDS loading buffer, and the samples were boiled for 5 min. The samples were then fractionated on SDS-PAGE and transferred to a polyvinylidene difluoride membrane, followed by autoradiograph or immunoblotting.

Single B cell culture

Single B cells were cultured in the presence of NB-21.2D9 feeder cells, provided by Dr. Garnett Kelsoe from Duke University (45). NB-21.2D9 cells were seeded into 96-well plates at a density of 1000 cells per 100 μl/well in B cell medium (RPMI 1640 supplemented with 10% FBS, 55 μM 2-ME, 100 U/ml penicillin, 100 μg/ml streptomycin, 10 mM HEPES, 1 mM sodium pyruvate, and 1% MEM nonessential amino acid). On the next day (day 0), recombinant mouse IL-4 (4 ng/ml, 100 μl/well; PeproTech) was added to the cultures, and single B cells were then sorted directly into each well using a BD FACSAria cell sorter. On day 2, 100 μl of culture medium was removed from the cultures and 200 μl of fresh B cell medium was added. From days 3 to 8, two-thirds of the culture medium (200 μl) was replaced with fresh B cell medium every day. On day 10, the culture supernatants were harvested and total IgG levels were determined by ELISA. Additionally, autoreactivity against nuclear and cytoplasmic self-antigens was determined by QUANTA Lite antinuclear Ab (ANA) ELISA (Inova Diagnostics).

High-throughput RNA sequencing and transcriptome analysis

Total RNA was extracted from sorted B cells using TRIzol, and mRNA was purified from the total RNA (10 to 50 ng) using a NEBNext poly(A) mRNA magnetic isolate module (New England Biolabs). Libraries were constructed from the purified mRNA using a NEBNext ultra RNA library prep kit for Illumina (New England Biolabs). The libraries were quantified using a Qubit fluorometer and KAPA library quantification kit. The average size of the libraries was determined using the D1000 ScreenTape system (Agilent Technologies) with a region selection of 150–900 bp. An equal molar amount of individual libraries from each sample was mixed and a total library of 1.7 pmol was then sequenced using an Illumina NextSeq 500 with aa NextSeq 500/550 v2 kit.

The sequenced libraries were demultiplexed and aligned to the *Mus musculus* mm10 genome using Basepair Tech (https://www.basepairtech.com) to quantify gene expression. The RNA sequencing (RNA-seq) libraries were normalized, and differential gene expression between samples was determined using DESeq2 v1.24.0 (46). Wald tests were used to determine whether fold changes were statistically significant. For visualization, the data were transformed using the regularized logarithm transformation (46) and batch effects were removed using the removeBatchEffect function from the limma v3.40.6 R package (47). Preranked gene set enrichment analysis (GSEA) was conducted using shrunken fold changes and the clusterProfiler v3.12.0 R package (48). The KEGG (49) and Reactome (50) databases were used as the reference sets. The Benjamini–Hochberg method was used to adjust *p* values for false discovery in both differential expression and GSEA (51).

Primers for quantitative real-time PCR

The following primer pairs were used for quantitative real-time PCR: β-actin forward, 5′-CCACAGCTGAGAGGGAAATC-3′, reverse, 5′-CTTCTCCAGGGAGGAAGAGG-3′; Card19 forward, 5′-TGACCTCCTGAGCCATCTACA-3′, reverse, 5′-TCTGCAATCTGAGTTTTGAGGAGA-3′.

Bm12 splenocyte-induced SLE autoimmune mouse model

Splenocytes (1×10^7) from age- and sex-matched Bm12 mice were adoptively transferred into B6.SJL-CD45.1 recipient mice that had been transplanted with BM cells from wild-type or CARD19-deficient mice. PBS alone, without any Bm12 splenocytes, was injected as a negative control. Three weeks after the adoptive transfer, sera were collected for autoantibody measurement using the QUANTA Lite ANA ELISA kit (Inova Diagnostics) and ANA test kit with HEp-2 cell–coated slides (Antibodies Incorporated). The mice were then sacrificed for flow cytometry analysis.

ANA ELISA

The ANA ELISA assay was performed according to the manufacturer's instructions. The kit included high-positive, low-positive, and negative controls. To ensure accuracy, the prediluted ANA ELISA high-positive control must have an absorbance >1.0, whereas the prediluted ANA negative control absorbance cannot be >0.15. The ANA ELISA low-positive absorbance must be more than twice the ELISA negative control or >0.15. The OD for each sample was first determined, then the reactivity for each sample was calculated by dividing the OD of each sample by the average OD of the ANA ELISA low positive. The result was multiplied by the number 25 of the units assigned to the ANA ELISA low positive by the kit. This was formulated as follows: Sample value (units) = sample OD/ANA ELISA low positive OD × ANA ELISA low positive (units 25).

Statistical analysis

Statistical analysis was performed using either a two-tailed unpaired Student *t* test for datasets with normal distribution or a Mann–Whitney *U* test for datasets with random distribution. The normality of all the data were analyzed using the D'Agostino and Pearson omnibus normality test using GraphPad Prism software.

Results

CARD19 interacts with TAK1 and inhibits TAK1 kinase activity

The overexpression of CARD19 has been reported to suppress BCL10-mediated activation of NF-κB (40). Our study aimed to uncover the molecular mechanism by which CARD19 regulates CBM-mediated activation of NF-κB. To achieve this, we examined the interactions of CARD19 with key components of the CBM-mediated NF-κB pathway, such as CARMA1, BCL10, MALT1, TRAF6, NEMO, TAK1, TAB1, and TAB2. MYC-tagged mouse CARD19 was coexpressed with FLAG-tagged mouse CARMA1, BCL10, MALT1, TRAF6, NEMO, or TAK1, or hemagglutinin-tagged mouse TAB1 or TAB2 in HEK293T cells. CARD19 had a strong interaction with TAK1 but weakly bound to TAB2, as demonstrated by its robust coimmunoprecipitation (co-IP) with TAK1 but moderate co-IP with TAB2 (Fig. 1A, 1B). Importantly, the reciprocal co-IP analysis showed that TAK1 but not TAB2 could associate with CARD19 (Fig. 1A, 1B). CARD19 also interacted with CARMA1, but not BCL10 or MALT1, as evidenced by its co-IP with CARMA1 but not with BCL10 or MALT1 (Supplemental Fig. 1A), and it interacted with TRAF6 and IκB kinase γ-subunit NEMO, as shown by its co-IP with TRAF6 (Supplemental Fig. 1B)

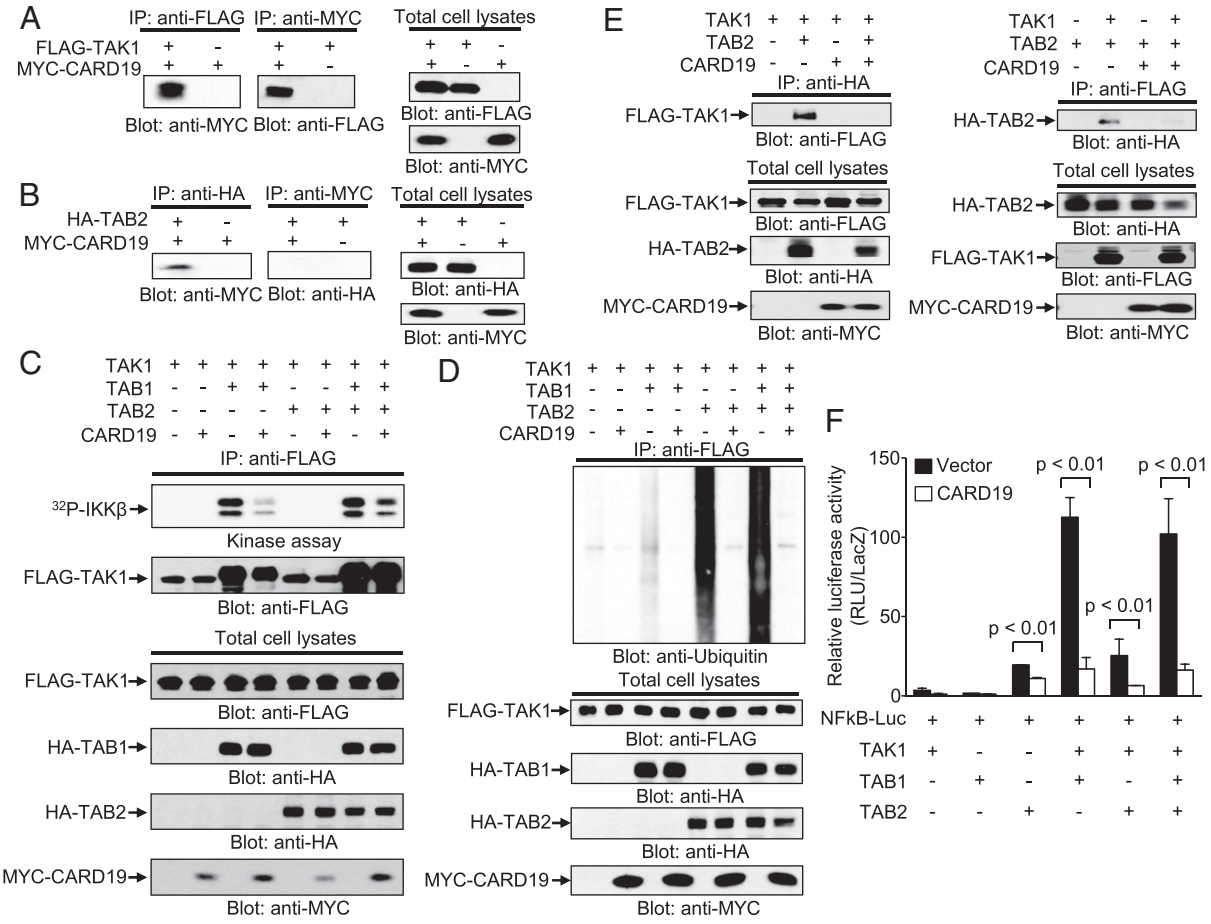

FIGURE 1. CARD19 interacts with TAK1 and inhibits TAK1 kinase activity. (**A** and **B**) Co-IP and reciprocal co-IP of CARD19 with TAK1 but not TAB2. HEK293T cells were transfected with the indicated plasmids encoding the indicated proteins for 48 h. Cell lysates were immunoprecipitated with the indicated Abs, and the immunoprecipitates were analyzed by immunoblotting with the indicated Abs. Total cell lysates (input) were analyzed by immunoblotting with the indicated Abs. (**C**) Inhibition of TAK1 kinase activity by CARD19. HEK293T cells were transfected with indicated plasmids encoding the indicated proteins for 48 h. Cells were lysed and TAK1 was immunoprecipitated with anti-FLAG, followed by an in vitro kinase assay using recombinant IKKβ as substrate. The remaining cell lysates were treated with λ phosphatase and then the expression of TAK1, TAB1, TAB2, and CARD19 in total cell lysates was analyzed by immunoblotting with the indicated Abs. (**D**) Inhibition of TAB2-induced TAK1 polyubiquitination by CARD19. HEK293T cells were transfected with the indicated plasmids encoding the indicated proteins for 48 h. Cells were lysed and TAK1 was immunoprecipitated with anti-FLAG, followed by immunoblotting with anti-ubiquitin Ab. Total cell lysates (input) were treated with λ phosphatase and then analyzed by immunoblotting with the indicated Abs. (**E**) Blockade of TAK1 and TAB2 interaction by CARD19. HEK293T cells were transfected with indicated plasmids encoding the indicated proteins for 48 h. Cell lysates were immunoprecipitated with the indicated Abs and the immunoprecipitates were analyzed by immunoblotting with the indicated Abs. Total cell lysates (input) were analyzed by immunoblotting with the indicated Abs. (**F**) Inhibition of TAK1-induced NF-κB activation by CARD19. HEK293T cells were transfected with indicated plasmids encoding the indicated proteins for 48 h. Luciferase activities in cell lysates were measured and β-galactosidase was used as an internal control. Mean ± SD is shown. The *p* values shown were calculated with an unpaired two-tailed Student *t* test. Data shown are representative of three independent experiments (A–F).

and NEMO (Supplemental Fig. 1C). However, reciprocal co-IP analysis showed that CARMA1, TRAF6, or NEMO could not associate with CARD19 (Supplemental Fig. 1). These co-IP and reciprocal co-IP data demonstrate that CARD19 has a strong interaction with TAK1 among the different key components of the CBM-mediated NF-κB pathway.

We next examined whether the strong interaction of CARD19 and TAK1 could affect TAK1 kinase activity. FLAG-tagged TAK1 was coexpressed without or with TAB1 or TAB2 alone or both in the presence or absence of CARD19 in HEK293T cells. TAK1 was isolated by IP, followed by an in vitro kinase assay using purified recombinant IKKβ as the substrate. As expected, TAK1 alone or with TAB2 did not phosphorylate IKKβ (Fig. 1C). In contrast, TAK1 in combination with TAB1 or both TAB1 and TAB2 strongly phosphorylated IKKβ (Fig. 1C). Notably, when CARD19 was present, the phosphorylation of IKKβ by TAK1 in combination with TAB1 or both TAB1 and TAB2 was markedly inhibited (Fig. 1C). These data demonstrate that CARD19 can suppress TAK1 kinase activity.

TAK1 is a ubiquitination-dependent kinase and its polyubiquitination is involved in its autoactivation (34). To examine the role of CARD19 in TAK1 ubiquitination, we studied the effect of TAB1 or TAB2 and CARD19 on TAK1 ubiquitination. As previous studies have shown (52), expression of TAB2 strongly induced TAK1 ubiquitination, whereas expression of TAB1 only slightly induced TAK1 ubiquitination (Fig. 1D). However, when CARD19 was coexpressed, it markedly abolished TAB2-mediated TAK1 ubiquitination (Fig. 1D). These data demonstrate that CARD19 can inhibit TAB2-mediated TAK1 ubiquitination.

Full activation of TAK1 kinase activity depends on its association with the regulatory subunits TAB1 and TAB2 (34, 52, 53). Interestingly, expression of CARD19 did not reduce the interaction of TAK1 with TAB1 (Supplemental Fig. 1D). In contrast, CARD19 completely blocked the association between TAK1 and TAB2 as

shown in co-IP and reciprocal co-IP assays (Fig. 1E). These data demonstrate that CARD19 can block the interaction between TAK1 and TAB2, thereby inhibiting TAB2-mediated TAK1 ubiquitination and activation.

Activation of TAK1 by the CBM complex through TAB1 and TAB2 ultimately leads to NF-κB activation (33, 35). Lastly, we examined the effect of CARD19 on TAK1-induced NF-κB activation. A NF-κB luciferase reporter plasmid was coexpressed with different combination of TAK1, TAB1, TAB2, and CARD19 in HEK293T cells. Subsequently, the luciferase activity, which reflects the NF-κB activation, was measured. TAK1 alone did not induce NF-κB activation (Fig. 1F). As expected, TAK1 together with TAB1, TAB2, or both strongly induced NF-κB activation (Fig. 1F). The strong activation of NF-κB by TAK1 plus TAB1 alone could be due to the presence of endogenous of TAB2 in HEK293T cells. Importantly, NF-κB activation by TAK1 plus TAB1, TAB2, or both was dramatically suppressed by the presence of CARD19 (Fig. 1F). Collectively, these data demonstrate that CARD19 negatively regulates TAK1 activity by preventing TAK1–TAB2 interaction, thus inhibiting TAK1 ubiquitination, activation, and subsequent NF-κB activation.

CARD19 deficiency has no effect on B cell development but suppresses autoimmunity

TAK1 is the key protein kinase in regulating NF-κB and plays an essential role in innate and adaptive immunity (32, 54–56). As the results have shown, CARD19 negatively regulates TAK1 kinase activity and subsequent NF-κB activation (Fig. 1). Thus, we sought to study the biological function of CARD19 in vivo by generating CARD19-deficient mice (Supplemental Fig. 1E–1G). We found that among the various hematopoietic compartments, CARD19 mRNA was ubiquitously expressed in different lymphoid populations, including B cells, T cells, and NK cells (Fig. 2A). CARD19 mRNA was also found to be highly expressed in granulocytes, macrophages, and dendritic cells (Fig. 2A). CARD19 mRNA was expressed in the different subsets of B cells and B cells at different developmental stages (Fig. 2A). In addition, CARD19 mRNA was found to be constitutively expressed in B cells before and after BCR engagement, whereas the control Bcl-x_L mRNA was clearly induced by BCR ligation (Fig. 2B). These results show that CARD19 is ubiquitously expressed in hematopoietic lineages and throughout B cell development.

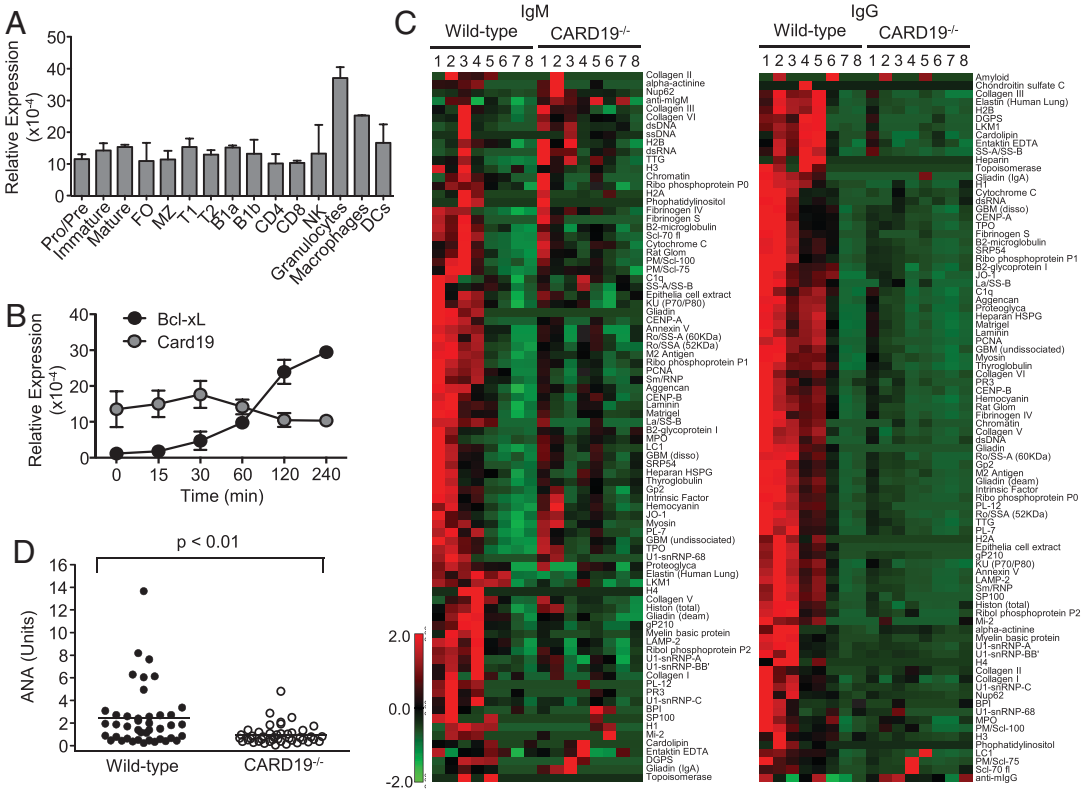

FIGURE 2. CARD19 is ubiquitously expressed and its deficiency suppresses autoantibody production in mice. (**A**) Expression of Card19 in different lymphoid and myeloid cell populations. Pro/pre, immature, and mature B cells, granulocytes, macrophages, and dendritic cells (DCs) were sorted from BM of wild-type mice; follicular (FO) and marginal zone (MZ) B cells, transitional type 1 (T1) and type 2 (T2) B cells, CD4 and CD8 T cells, and NK cells were sorted from the spleens of wild-type mice; and B1a and B1b cells were sorted from the peritoneal fluid of wild-type mice. Total RNAs were extracted from the cells, transcribed into cDNA, and Card19 mRNA levels were quantified by quantitative real-time PCR analysis, using β-actin as an internal control. Mean ± SD is shown. (**B**) Constitutive expression of CARD19 mRNA in splenic B cells. Total splenic B cells were sorted from wild-type mice and then stimulated with anti-IgM for the indicated time. Total RNAs were extracted, transcribed into cDNA, and mRNA levels of Card19 and Bcl-x_L were quantified by quantitative real-time PCR analysis. Mean ± SD is shown. (**C**) Suppression of autoantibody production in CARD19-deficient mice. Sera from 2-mo-old wild-type and CARD19-deficient mice were subjected to a self-antigen array for detection of self-reactive IgM and IgG. Each column represents an individual mouse and each row represents an individual self-antigen. Red, green, and black grid blocks indicate expression above, below, and at the median of all samples at each row. (**D**) Increased frequency of self-reactive B cells in CARD19-deficient mice. Single splenic B cells were sorted from wild-type or CARD19$^{-/-}$ mice and cultured in 96-well plates that were preseeded with feeder cells. After 10 d of culture, total IgG levels in the supernatants from the single-cell cultures, 42 from wild-type mice and 43 from CARD19$^{-/-}$ mice, were determined, and autoreactivity was determined by ANA ELISA. Each dot represents a single B cell culture and horizontal lines represent the mean values. The *p* values were calculated with a Mann–Whitney *U* test. Data shown are representative of three (A and D) or two (B) independent experiments, or obtained from eight wild-type and CARD19$^{-/-}$ mice (C).

Although CARD19 was expressed in multiple hematopoietic lineages, CARD19-deficient mice surprisingly possessed normal populations of macrophages, granulocytes, erythrocytes, and NK cells in the BM of mutant mice (Supplemental Fig. 1H). Additionally, CARD19-deficient mice also exhibited normal populations of macrophages, granulocytes, erythrocytes, NK cells, and T cells in the spleens (Supplemental Fig. 1I, 1J). These results demonstrate that CARD19 deficiency has no detectable effect on hematopoiesis, including myeloid, erythroid, and lymphoid development. This suggests that although CARD19 is expressed throughout hematopoietic lineages and B cell development, it may not play a critical role in the overall development of these cells.

Furthermore, CARD19 deficiency did not impact B cell development and maturation, as evidenced by the presence of normal populations of various B cell subsets and B cells at the different developmental stages (Supplemental Fig. 2A–E). Populations of germinal center (GC) B cells were comparable between naive wild-type and CARD19-deficient mice (Supplemental Fig. 2F). Additionally, baseline levels of serum Ig were normal in CARD19-deficient mice (Supplemental Fig. 2G), and both T cell–dependent and T cell–independent immune responses were normal in CARD19-deficient relative to wild-type controls (Supplemental Fig. 2H, 2I). These data show that CARD19 deficiency does not affect B cell development or B cell immune response.

Dysregulation of the NF-κB signaling pathway caused by the deletion of a negative regulator can often lead to severe autoimmunity (17, 57–59). To assess the effect of CARD19 deficiency on B cell tolerance to self-antigen, we used a self-antigen array to screen for autoantibodies in the sera of 2-mo-old CARD19-deficient mice. Our results showed that CARD19-deficient mice displayed a marked decrease in self-reactive IgM and IgG compared with wild-type controls (Fig. 2C). Moreover, single splenic B cells were sorted from 2-mo-old CARD19-deficient mice or wild-type controls. After 10 d of culture, the total IgG levels in the supernatants from the single-cell cultures were determined and autoreactivity against nuclear and cytoplasmic self-antigens was determined by ANA ELISA. There were markedly fewer self-reactive single B cells detected in splenic B cells from CARD19-deficient relative to wild-type mice (Fig. 2D). These data indicate that CARD19 deficiency reduces autoimmunity in vivo.

CARD19 deficiency enhances B cell tolerance

The finding that CARD19 deficiency reduces autoantibody production in vivo suggests its role in B cell tolerance. To directly investigate the role of CARD19 in B cell tolerance, we bred CARD19-deficient mice with MD4/ML5 transgenic mice, which are a well-established B cell tolerance mouse model. In this model, Ig^{HEL} and sHEL mice were used (8). Clonal deletion of self-reactive B cells is a crucial mechanism for establishing B cell tolerance (4). The B cell population was reduced in the spleen of CARD19-deficient Ig^{HEL}sHEL double-transgenic mice compared with wild-type controls (Fig. 3A). This suggests that self-reactive CARD19-deficient B cells might undergo increased clonal deletion. Furthermore, a TUNEL assay revealed that self-antigen HEL or anti-IgM stimulation indeed increased apoptosis of B cells from CARD19-deficient Ig^{HEL}sHEL double-transgenic mice when compared with wild-type controls (Fig. 3B). These findings suggest that CARD19 deficiency augments self-antigen–induced cell apoptosis, resulting in more clonal deletion of autoreactive B cells and thus promoting B cell tolerance.

Receptor editing is another important mechanism for establishing B cell tolerance (6, 7). Ig^{HEL} transgenic mice bear a transgene encoding the κ L chain, and expression of the endogenous λ L chain is an indication of receptor editing (8). The frequency of λ L chain–positive splenic B cells was significantly increased in CARD19-deficient relative to wild-type Ig^{HEL}sHEL double-transgenic mice (Fig. 3C). This finding is consistent with increased endogenous λ L chain expression. HEL specificity was decreased in CARD19-deficient relative to wild-type Ig^{HEL}sHEL B cells, whereas the level of surface IgM was comparable between mutant and control B cells (Fig. 3D). These results demonstrate that the lack of CARD19 facilitates receptor editing of self-reactive B cells.

Self-reactive B cells can evade central tolerance and enter the periphery, where they constantly encounter self-antigens and become anergic. Anergic B cells are characterized by decreased cell proliferation, downregulation of activation markers, and impairment of BCR signaling (8, 60). B cells from wild-type Ig^{HEL}sHEL double-transgenic mice were anergic and displayed low proliferation rates upon self-antigen HEL stimulation, as evidenced by low BrdU incorporation (Fig. 3E). Strong BCR engagement through anti-IgM stimulation could enhance BrdU incorporation in wild-type anergic B cells (Fig. 3E). However, B cells from CARD19-deficient relative to wild-type Ig^{HEL}sHEL mice exhibited much less BrdU incorporation following self-antigen HEL or anti-IgM stimulations (Fig. 3E). Additionally, B cells from CARD19-deficient relative to wild-type Ig^{HEL}sHEL mice displayed markedly less ^{3}H-thymidine incorporation following self-antigen HEL or anti-IgM stimulations (Fig. 3F). These data demonstrate that CARD19 deficiency renders self-reactive B cells less proliferative in response to BCR engagement.

CD86 upregulation, an indicator of B cell activation (61), was further suppressed in CARD19-deficient Ig^{HEL}sHEL double-transgenic B cells after BCR engagement by HEL or anti-IgM stimulation (Fig. 3G). Anergic B cells are also characterized by low expression of CD23 (62). When compared with wild-type control B cells, CARD19-deficient Ig^{HEL}sHEL B cells expressed significantly lower levels of CD23 (Fig. 3H). This further supports the conclusion that CARD19-deficient self-reactive B cells have impaired ability to be activated upon BCR engagement.

BCR signaling, including ERK activation, is suppressed in anergic B cells (60). Self-antigen HEL moderately induced ERK activation in wild-type Ig^{HEL}sHEL B cells (Fig. 3I). In contrast, HEL completely failed to induce ERK activation in CARD19-deficient Ig^{HEL}sHEL B cells (Fig. 3I). It is noteworthy that the activation of other signaling pathways was barely detected in wild-type and CARD19-deficient Ig^{HEL}sHEL B cells. Taken together, these findings demonstrate that CARD19 plays a role in regulating B cell tolerance and its deficiency leads to an increase in clonal deletion, receptor editing, and anergy of self-reactive B cells.

CARD19 deficiency enhances the expression of Cbl and Egr in B cells

The negative regulators of BCR signaling play a crucial role in regulating B cell tolerance (17, 57–59). Our findings show that CARD19 deficiency affects the response of self-reactive B cells to BCR engagement. To investigate the molecular mechanism by which CARD19 regulates B cell tolerance, we studied the effect of CARD19 deficiency on the expression of BCR signaling negative regulators in naive B cells. B cells from CARD19-deficient and control Ig^{HEL} single-transgenic mice were purified and stimulated with HEL in vitro. We found that after long-term stimulation, BCR induced a higher expression of the two members of the E3 ubiquitin ligases, c-Cbl and Cbl-b, in CARD19-deficient relative to wild-type Ig^{HEL} B cells (Fig. 4A). It is noteworthy that the similar low basal levels of c-Cbl and Cbl-b were detected in B cells from CARD19-deficient and wild-type single-transgenic Ig^{HEL} mice (Fig. 4A). In contrast, the expression levels of the protein phosphatase Shp1 were comparable between CARD19-deficient and wild-type Ig^{HEL} B cells before and after BCR engagement by HEL stimulation (Fig. 4A). Additionally, the expression of control PLCγ2 or actin was comparable between mutant and wild-type Ig^{HEL} B cells

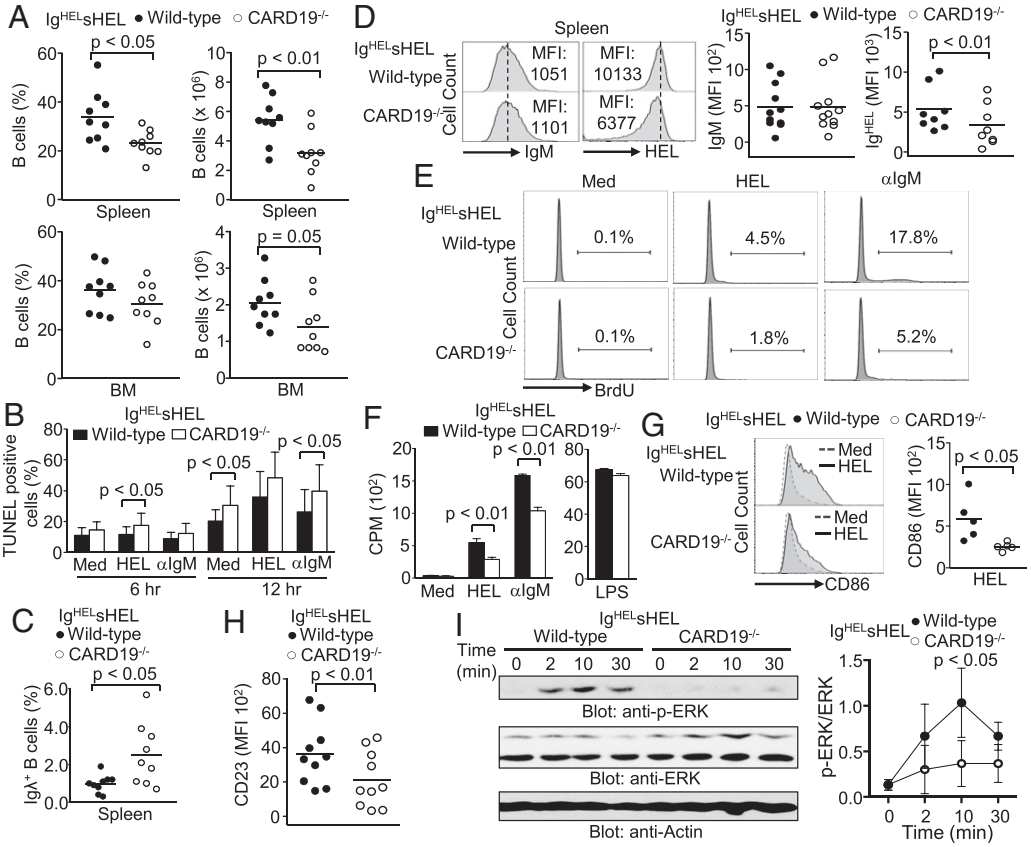

FIGURE 3. CADR19 deficiency enhances B cell tolerance. (**A**) Reduction of B cell population in CARD19-deficient Ig^{HEL}sHEL mice. Splenocytes and BM cells from wild-type and CARD19$^{-/-}$ Ig^{HEL}sHEL mice were stained with anti-B220 Abs. Percentages and total numbers of B cells in wild-type and CARD19-deficient Ig^{HEL}sHEL double-transgenic mice were determined. (**B**) Increased apoptosis of self-reactive B cells in CARD19-deficient Ig^{HEL}sHEL mice. Splenic B cells isolated from wild-type and CARD19$^{-/-}$ Ig^{HEL}sHEL mice were stimulated with medium (Med), HEL, or anti-IgM (αIgM) for the indicated time points and cell apoptosis was detected by a TUNEL assay. (**C**) Increased Igλ$^+$ B cells in CARD19-deficient Ig^{HEL}sHEL mice. Splenocytes from wild-type and CARD19$^{-/-}$ Ig^{HEL}sHEL mice were stained with anti-B220 and anti-Igλ. Percentages indicate Igλ$^+$ B cells in the gated splenic B220$^+$ population. (**D**) Reduced HEL specificity of B cells in CARD19-deficient Ig^{HEL}sHEL mice. Splenocytes from wild-type and CARD19$^{-/-}$ Ig^{HEL}sHEL mice were stained with fluorescent-conjugated Ag HEL or anti-IgM. The mean fluorescence intensity (MFI) was quantified. (**E**) Lower BCR-induced incorporation of BrdU in B cells from CARD19-deficient Ig^{HEL}sHEL mice. Splenic B cells purified from wild-type and CARD19$^{-/-}$ Ig^{HEL}sHEL mice were cultured in the presence of Ag HEL or anti-IgM for 48 h. Cells were pulsed with BrdU and BrdU$^+$ B cells were analyzed by FACS. (**F**) Lower BCR-induced ^{3}H-thymidine incorporation in B cells from CARD19-deficient Ig^{HEL}sHEL mice. Splenic B cells purified from wild-type and CARD19$^{-/-}$ Ig^{HEL}sHEL mice were cultured in the presence of Ag HEL or anti-IgM for 48 h. Cells were pulsed with ^{3}H-thymidine and radioactivity was measured. (**G**) Decreased upregulation of CD86 in B cells from CARD19-deficient Ig^{HEL}sHEL mice. Splenic B cells from wild-type and CARD19$^{-/-}$ Ig^{HEL}sHEL mice were incubated with Ag HEL for 24 h. The upregulation of CD86 was measured by FACS. (**H**) Reduced expression of CD23 on B cells from CARD19-deficient Ig^{HEL}sHEL mice. Expression of activation marker CD23 on splenic B cells from wild-type and CARD19$^{-/-}$ Ig^{HEL}sHEL mice were analyzed by FACS. (**I**) Further reduced activation of ERK in B cells from CARD19-deficient Ig^{HEL}sHEL mice. Splenic B cells from wild-type and CARD19$^{-/-}$ Ig^{HEL}sHEL mice were stimulated with Ag HEL for the indicated time. Cells were lysed and analyzed by immunoblot with the indicated Abs (left panel). Band intensity of p-ERK and ERK was measured using ImageJ software, and the results from three experiments are presented as a ratio of the band intensity of p-ERK to total ERK (right panel). Each dot represents an individual mouse and horizontal lines represent the mean values. MFI was quantified and mean ± SD is shown. The *p* values shown were calculated with an unpaired two-tailed Student *t* test. Data shown are obtained from 9 (A and C), 8 (D), 5 (G), or 10 (H) wild-type Ig^{HEL}sHEL mice and 9 (A and C), 8 (D), 5 (G), or 10 (H) CARD19$^{-/-}$ Ig^{HEL}sHEL mice, or representative of 5 (B and F), 4 (E), or 3 (I) independent experiments.

before and after BCR engagement (Fig. 4A). c-Cbl and Cbl-b control BCR-mediated B cell anergy, and deletion of both c-Cbl and Cbl-b in B cells leads to SLE-like autoimmunity (17). These data show that CARD19 deficiency increases BCR-induced but not basal expression of c-Cbl and Cbl-b in naive B cells.

The transcription factors Egr2 and Egr3 are known to regulate the expression of Cbl-b in T cells (63). Our results showed that compared with wild-type control cells, CARD19-deficient Ig^{HEL} B cells expressed markedly higher HEL stimulation-induced Egr2 and Egr3 but not basal levels (Fig. 4A). Of note, the expression of PLCγ2 or actin was comparable between mutant and wild-type Ig^{HEL} B cells before and after BCR engagement (Fig. 4A). Therefore, CARD19 deficiency elevates BCR-induced but not basal expression of Egr2 and Egr3 in naive B cells.

Next, we examined the effect of CARD19 deficiency on basal and BCR-induced expression of c-Cbl/Cbl-b and Egr2/3 in self-reactive B cells. B cells from CARD19-deficient and control Ig^{HEL}sHEL double-transgenic mice were purified and stimulated with HEL in vitro. Our results showed that the basal levels of c-Cbl and Cbl-b were increased in B cells of CARD19-deficient relative to wild-type double-transgenic Ig^{HEL}sHEL mice (Fig. 4B). Additionally, upon in vitro HEL stimulation, both c-Cbl and Cbl-b proteins were elevated much more in CARD19-deficient relative to wild-type Ig^{HEL}sHEL B cells (Fig. 4B). Furthermore, CARD19-deficient Ig^{HEL}sHEL B cells expressed markedly higher basal and HEL stimulation-induced levels of Egr2 and Egr3 when compared with wild-type control cells (Fig. 4B). In contrast, the expression levels of Shp1, PLCγ2, or actin were comparable between CARD19-deficient and wild-type

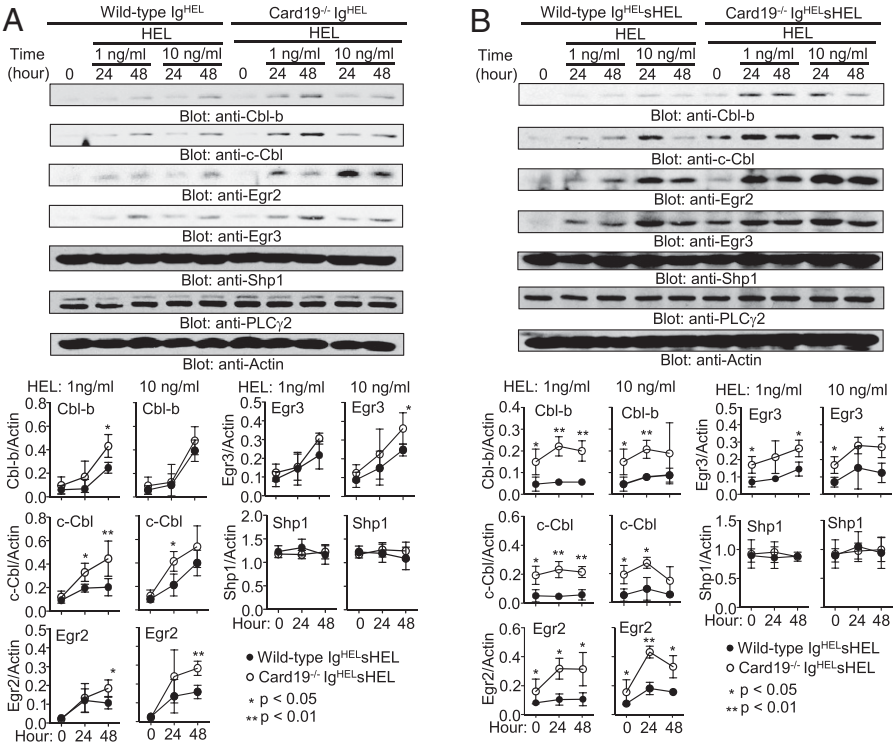

FIGURE 4. CARD19 deficiency elevates the expression of c-Cbl/Cbl-b and Egr2/3 in B cells. (**A**) Elevation of BCR-induced expression of c-Cbl/Cbl-b and Egr2/3 in CARD19-deficient B cells. Splenic B cells from wild-type and CARD19$^{-/-}$ Ig^{HEL} single-transgenic mice were cultured in the presence of HEL for the indicated time. The cell lysates were analyzed by immunoblotting with the indicated Abs. (**B**) Elevation of basal and BCR-induced expression of c-Cbl/Cbl-b and Egr2/3 in CARD19-deficient self-reactive B cells. Splenic B cells from wild-type and CARD19$^{-/-}$ Ig^{HEL}sHEL double-transgenic mice were cultured in the presence of the self-antigen HEL for the indicated time. The cell lysates were analyzed by immunoblotting with the indicated Abs. The intensities of protein bands were quantified using ImageJ software. The *p* values shown were calculated with an unpaired two-tailed Student *t* test. Mean ± SD is shown. Data shown are representative of three independent experiments (A and B).

Ig^{HEL}sHEL B cells before and after BCR engagement by HEL stimulation (Fig. 4B). The markedly increased basal expression of c-Cbl/Cbl-b and Egr2/3 in self-reactive B cells is consistent with the finding that self-antigen HEL failed to rapidly induce ERK activation in CARD19-deficient self-reactive B cells (Fig. 3I). Taken together, these data suggest that CARD19 deficiency increases basal and BCR-induced expression of c-Cbl/Cbl-b and Egr2/3 in self-reactive B cells, which could account for enhanced anergy.

NF-κB activation by CARD19 deficiency results in increased expression of Cbl and Egr

CARD19 regulated NF-κB signaling through its interaction with TAK1 in the overexpression system (Fig. 1). Therefore, we sought to confirm that CARD19 regulated NF-κB activation in naive B cells from Ig^{HEL} single-transgenic mice. Consistent with the finding that CARD19 deficiency had no effect on B cell development (Supplemental Fig. 2A–E), B cell frequency and number were normal in CARD-deficient relative to wild-type Ig^{HEL} single-transgenic mice (Supplemental Fig. 3A). Additionally, surface IgM level was normal in CARD19-deficient Ig^{HEL} B cells (Supplemental Fig. 3B). Splenic B cells from CARD19-deficient or wild-type Ig^{HEL} single-transgenic mice were isolated and stimulated with HEL. BCR-induced IκBα phosphorylation was increased in CARD19-deficient relative to wild-type Ig^{HEL} B cells (Fig. 5A), indicating that NF-κB activation was enhanced in CARD19-deficient primary B cells. In contrast, BCR-induced phosphorylation of AKT, p38, JNK, or ERK was comparable between CARD19-deficient and wild-type Ig^{HEL} B cells (Fig. 5B). Furthermore, we examined NF-κB activation by the gel shift assay. After HEL stimulation, NF-κB activation was markedly enhanced in CARD19-deficient relative to wild-type Ig^{HEL} B cells (Fig. 5C). In contrast, activation of AP-1 was comparable between CARD19-deficient and wild-type Ig^{HEL} B cells (Fig. 5C). These data demonstrate that BCR-induced NF-κB activation is augmented in CARD19-deficient primary naive B cells.

Moreover, we sought to determine whether the enhanced BCR-induced NF-κB activation in CARD19-deficient B cells was responsible for the increased expression of Cbl and Egr. Splenic naive B cells were isolated from wild-type mice and then stimulated with anti-IgM, phorbol 12,13-dibutyrate (PDBu), or ionomycin. PDBu, a phorbol ester, activates PKC and subsequently leads to NF-κB activation, whereas ionomycin initiates Ca^{2+} release and subsequently results in NFAT activation (64). PDBu, similar to anti-IgM, was able to induce the expression of c-Cbl and Egr2 in wild-type B cells (Fig. 5D, 5E). However, ionomycin alone failed to induce the expression of Cbl or Egr in wild-type B cells (Fig. 5D, 5E). These data indicate that the PKC/NF-κB pathway, but not Ca^{2+}/NFAT pathway, is responsible for BCR-induced expression of Cbl and Egr in B cells, which is a distinct mechanism from that for T cells (65, 66).

We further sought to prove that NF-κB activation is required for BCR-induced expression of Cbl and Egr in B cells. To do this, we used c-Rel–deficient mice as a model system, as c-Rel is a critical NF-κB subunit and its deficiency impairs NF-κB activation in B cells (67). Splenic B cells from wild-type and c-Rel–deficient mice were isolated and then activated by anti-IgM stimulation. Compared to medium alone or IL-4 stimulation, BCR engagement induced the expression of Cbl and Egr in wild-type but not in c-Rel–deficient B cells (Fig. 5F, 5G). Interestingly, BCR-induced expression of NFATc1 was not affected by c-Rel deficiency (Fig. 5F, 5G). Additionally, the expression of PLCγ2 or actin was comparable between wild-type and c-Rel–deficient B cells before and after BCR engagement (Fig. 5F, 5G). Taken together, these data demonstrate that the enhanced activation of NF-κB by CARD19 deficiency is responsible for increased expression of Cbl and Egr upon BCR engagement in B cells.

CARD19 deficiency enhances hyporesponsiveness of self-reactive anergic B cells

To further determine the effect of enhanced BCR-induced NF-κB activation by CARD19 deficiency on naive B cells, we employed a high-throughput RNA-seq approach to examine the global gene expression profile of wild-type and mutant naive B cells following BCR engagement. Splenic B cells from wild-type and CARD19-

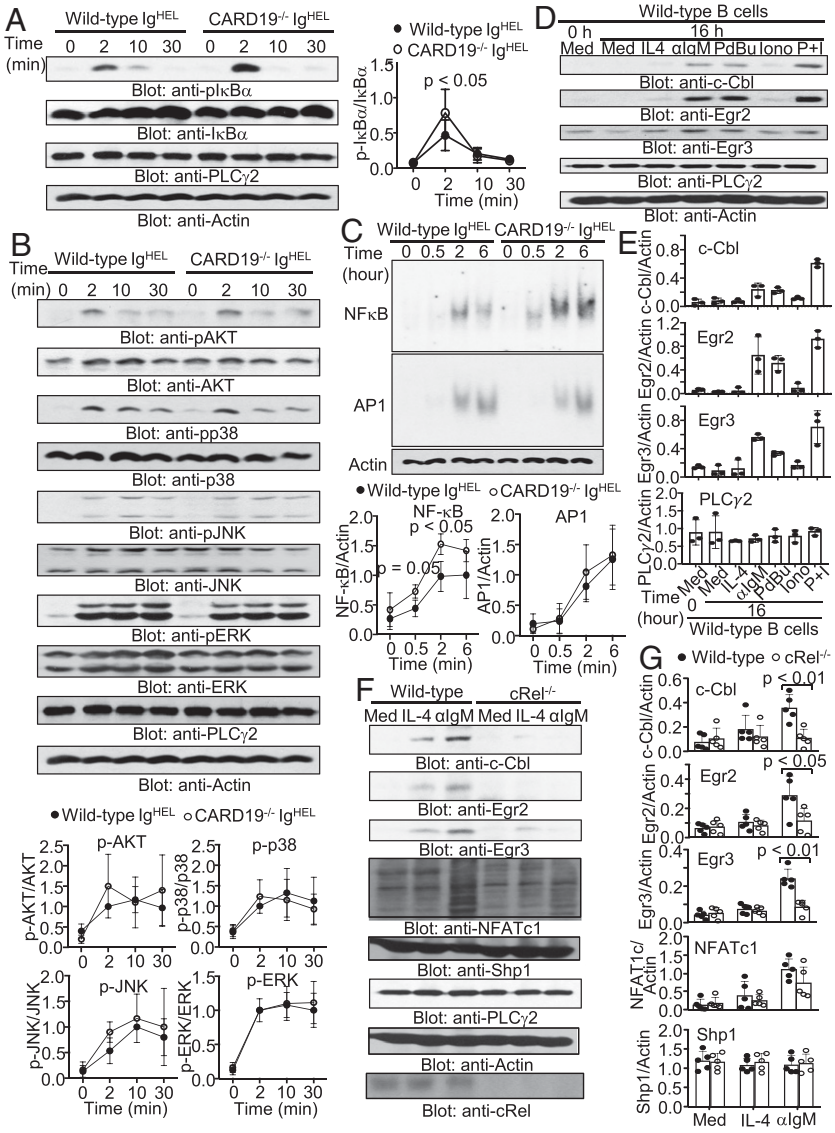

FIGURE 5. CARD19 deficiency enhances BCR-induced NF-κB activation that regulates the expression of c-Cbl/Cbl-b and Egr2/3 in B cells. (**A** and **B**) Enhancement of BCR-induced IκBα phosphorylation but not other pathway activation in CARD19-deficient B cells. Splenic B cells from wild-type and CARD19$^{-/-}$ Ig^{HEL} mice were stimulated with HEL for the indicated time. The cell lysates were analyzed by immunoblotting with the indicated Abs (left panel). Band intensity was measured using ImageJ software, and the results from six (A) or three (B) experiments are presented as a ratio of the band intensity of phosphoprotein to total protein (right panel). (**C**) Enhancement of BCR-induced NF-κB activation in CARD19-deficient B cells. Splenic B cells from wild-type and CARD19$^{-/-}$ Ig^{HEL} mice were stimulated with HEL for the indicated time. The cell lysates were analyzed for NF-κB and AP-1 activation using the gel shift assay, and actin expression was used as a loading control (left panel). Band intensity was measured using ImageJ software, and the results from four experiments are presented as a ratio of the band intensity of NF-κB or AP-1 to actin (right panel). (**D**) PKC-induced NF-κB activation controls the expression of c-Cbl/Cbl-b and Egr2/3 in B cells. Splenic B cells from wild-type mice were cultured with medium alone (Med), IL-4 alone (IL-4), or in the presence of anti-IgM (αIgM), PDBu, ionomycin, or PDBu plus ionomycin (P + I) for 16 h. The cell lysates were analyzed by immunoblotting with the indicated Abs. (**E**) Quantification of the intensities of protein bands in (D) using ImageJ software. The results from three experiments are presented as a ratio of the band intensity of c-Cbl, Egr2, Egr3, or PLCγ2 to actin. (**F**) The NF-κB subunit c-Rel is required for BCR-induced expression of c-Cbl/Cbl-b and Egr2/3 in B cells. Splenic B cells from wild-type or c-Rel$^{-/-}$ mice were cultured with medium alone (Med), IL-4 alone (IL-4), or in the presence of anti-IgM (αIgM) for 16 h. The cell lysates were analyzed by immunoblotting with the indicated Abs. (**G**) Quantification of the intensities of protein bands in (E) using ImageJ software. The results from five experiments are presented as a ratio of the band intensity of c-Cbl, Egr2, Egr3, or PLCγ2 to actin. Mean ± SD is shown. The *p* values shown were calculated with an unpaired two-tailed Student *t* test. Data shown are representative of six (A), three (B), four (C), three (D and E), or five (F and G) independent experiments.

deficient Ig^{HEL} single-transgenic mice were sorted, stimulated with the Ag HEL, and then subjected to high-throughput RNA-seq. The principal component analysis (PCA) of transcripts showed that replicates of unstimulated wild-type and CARD19-deficient Ig^{HEL} B cells clustered together, showing that gene expression profiles of wild-type and CARD19-deficient naive B cells without Ag stimulation were similar (Fig. 6A). Additionally, replicates of HEL-stimulated wild-type and CARD19-deficient Ig^{HEL} B cells also clustered together, demonstrating that gene expression profiles of wild-type and CARD19-deficient naive B cells after Ag stimulation were comparable as well (Supplemental Fig. 3C). Differential expression analysis demonstrated that HEL-stimulated wild-type Ig^{HEL} B cells displayed a marked change in their gene expression profile compared with unstimulated wild-type Ig^{HEL} B cells (Supplemental Fig. 3D, 3E). Similarly, a substantial change in the gene expression profile was observed in HEL-stimulated relative to unstimulated CARD19-

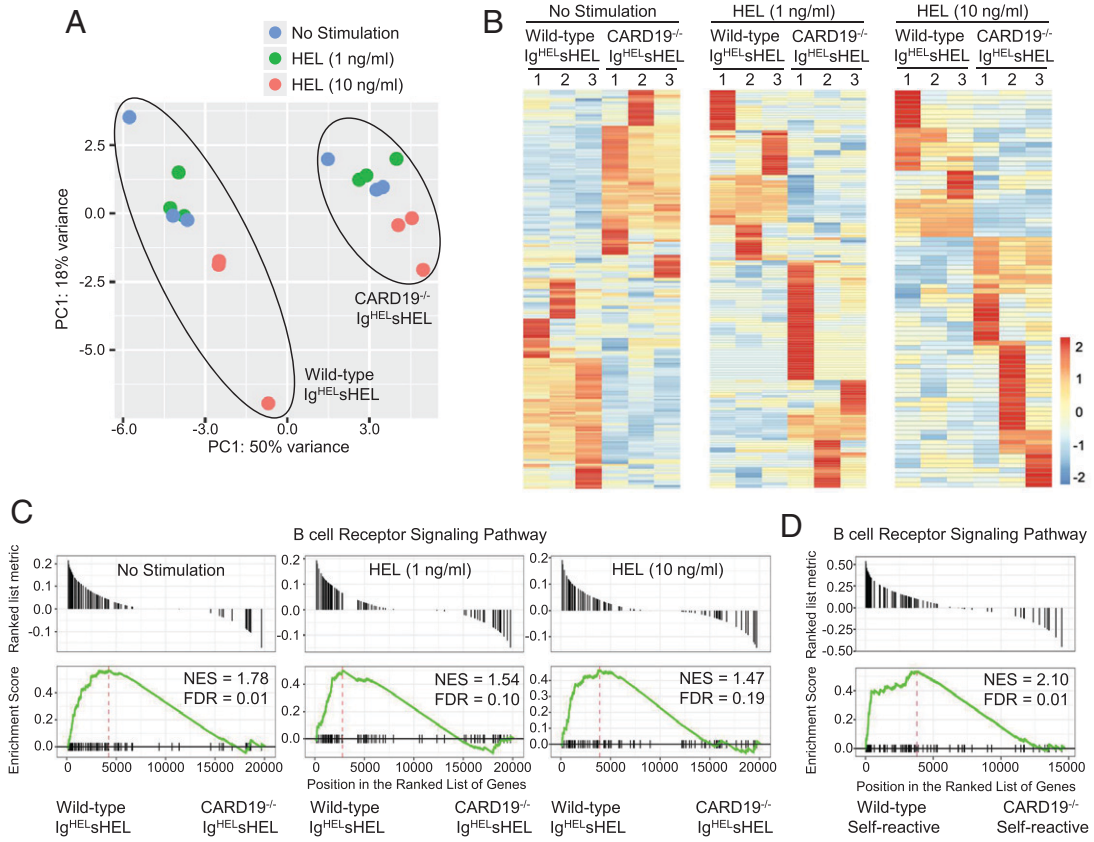

FIGURE 6. CARD19 deficiency affects the gene expression profile of self-reactive B cells. (**A–C**) Splenic self-reactive anergic B cells from wild-type and CARD19-deficient Ig^{HEL}sHEL mice were stimulated without or with the indicated concentration of HEL for 24 h and then subjected to high-throughput RNA-seq. The transcriptome profiles were analyzed. (A) Principal component analysis (PCA) of wild-type and CARD19-deficient Ig^{HEL}sHEL B cells without and with HEL stimulation. (B) Heatmap of differentially expressed genes in wild-type and CARD19-deficient Ig^{HEL}sHEL B cells without and with (C) HEL stimulation and upregulated or downregulated genes with adjusted $p < 0.05$. Comparative GSEA of the BCR signaling pathway target gene signatures in self-reactive B cells of wild-type and CARD19-deficient Ig^{HEL}sHEL mice. (**D**) Comparative GSEA of the BCR signaling pathway target gene signatures in self-reactive anergic B cells of wild-type and CARD19-deficient mice. Self-reactive anergic B cells from wild-type and CARD19-deficient mice were sorted and subjected to high-throughput RNA-seq. Data shown were obtained from three wild-type or CARD19-deficient Ig^{HEL}sHEL mice (A–C) and from three wild-type or CARD19-deficient mice (D).

deficient Ig^{HEL} B cells (Supplemental Fig. 3D, 3E). Importantly, Ag stimulation-induced changes in the gene expression profiles were found to overwhelmingly overlap between wild-type and CARD19-deficient Ig^{HEL} B cells (Supplemental Fig. 3F, 3G). This observation was consistent with the finding that the rates of BCR-induced ^{3}H-thymidine incorporation of B cells from wild-type and CARD19-deficient Ig^{HEL} mice were comparable (Supplemental Fig. 3H). Additionally, CARD19 deficiency had no effect on B cell development or B cell immune response (Supplemental Fig. 2). Taken together, these results demonstrate that the enhanced activation of NF-κB by CARD19 deficiency does not affect the overall Ag-induced gene expression and functions of naive B cells.

We next examined the effect of enhanced BCR-induced NF-κB activation by CARD19 deficiency on self-reactive B cells. B cells isolated from wild-type and CARD19-deficient Ig^{HEL}sHEL double-transgenic mice were stimulated with the Ag HEL and then subjected to the high-throughput RNA-seq analysis. In contrast to our finding in naive B cells, PCA of transcripts showed that replicates of wild-type and CARD19-deficient Ig^{HEL}sHEL B cells clustered separately, indicating that the gene expression profiles of wild-type and CARD19-deficient Ig^{HEL}sHEL B cells with or without Ag stimulation were distinct (Fig. 6A). Differential expression analysis revealed that unstimulated CARD19-deficient Ig^{HEL}sHEL B cells displayed a markedly different gene expression profile compared with unstimulated wild-type control B cells (Fig. 6B). Furthermore, the gene expression profile was distinct in HEL-stimulated CARD19-deficient relative to wild-type Ig^{HEL}sHEL B cells (Fig. 6B). GSEA demonstrated that the BCR signaling pathway-targeted genes were enriched in wild-type relative to CARD19-deficient self-reactive B cells in the absence or presence of HEL stimulation (Fig. 6C), further confirming that CARD19 deficiency suppresses BCR signaling. To provide additional support, we further confirmed that CARD19 deficiency results in hyporesponsiveness in self-reactive B cells by examining the global gene expression of wild-type and mutant self-reactive B cells isolated from nontransgenic wild-type and CARD19-deficient mice. A marker set that has been used to classify late-transitional (T3) B cells actually identifies self-reactive anergic B cells within wild-type B cell compartments (10). Self-reactive anergic B cells (B220^{+}AA4.1^{+}CD23^{+}IgM^{lo}) were sorted from wild-type and CARD19-deficient nontransgenic mice and subjected to the high-throughput RNA-seq analysis. GSEA results confirmed that the BCR signaling pathway-targeted genes were enriched in wild-type relative to CARD19-deficient self-reactive anergic B cells (Fig. 6D). These global gene expression profiling results were consistent with our findings that CARD19-deficient self-reactive B cells had increased basal and BCR-induced expression of c-Cbl/Cbl-b and Egr2/3 (Fig. 4B) and exhibited enhanced anergy, as evidenced by reduced Ag-induced proliferation (Fig. 3E, 3F), activation (Fig. 3G, 3H), and ERK activation (Fig. 3I) following self-antigen

stimulation. Taken together, these data demonstrate that CARD19 deficiency enhances hyporesponsiveness of self-reactive B cells.

CARD19 deficiency prevents Bm12-induced SLE

To investigate the biological significance of enhanced tolerance caused by deficiency in CARD19, we examined its role in the development of SLE using a mouse model. SLE is an autoimmune disease with a wide range of clinical and immunological manifestations (68). The Bm12 transfer model is a commonly used mouse model for SLE that mimics the characteristics of human SLE, such as splenomegaly, ANA production, and the expansion of GC B cells (69). In this model, lymphocytes from Bm12 mice are adoptively transferred into C57BL/6 mice, leading to alloactivation of donor CD4 T cells by recipient APCs and the subsequent production of autoantibodies and SLE-like symptoms (69). We transplanted B6.SJL-CD45.1 mice with BM cells from wild-type or CARD19-deficeint mice, which were on a C57BL/6 genetic background. Eight weeks after transplantation, we adoptively transferred Bm12 splenocytes into the recipients. Three weeks after adoptive transfer, wild-type BM recipients exhibited enlarged spleens with increased mass and cellularity compared with wild-type BM recipients that received PBS as control (Fig. 7A). However, recipients that received CARD19-deficient BM failed to display spleen enlargement compared with wild-type or CARD19-deficient BM recipient controls that received PBS (Fig. 7A). Additionally, recipients that received CARD19-deficient BM cells generated markedly less ANA IgG following Bm12 lymphocyte adoptive transfer, detected by ELISA (Fig. 7B) or HEp-2 immunofluorescence assay (Fig. 7C, 7D). An autoantigen array further confirmed the reduction of autoantibody production in CARD19-deficient BM recipients compared with wild-type BM recipients (Fig. 7E). Furthermore, flow cytometry analysis showed that the upregulation of the B cell activation marker CD86 was markedly attenuated in CARD19-deficient relative to wild-type BM recipients after adoptively transferring Bm12 splenocytes (Supplemental Fig. 4A). These results demonstrate that CARD19 deficiency can prevent the development of autoimmune disease.

To further determine whether the prevention of Bm12-induced SLE by CARD19 deficiency is due to intrinsic B cell defects, we generated BM chimeric mice with B cell–specific deletion of CARD19. BM cells from wild-type or CARD19-deficient mice were mixed with BM cells from B cell–deficient μMT mice and transplanted into lethally irradiated μMT mice. Single splenic B cells were sorted from the BM chimeric mice and cultured for 10 d. The levels of total IgG in the culture supernatants were determined and the presence of autoreactive Abs against nuclear and cytoplasmic self-antigens was determined by ANA IgG ELISA. Compared to BM chimeric mice with wild-type B cells, BM chimeric mice with B cell–specific deletion of CARD19 had markedly lower frequency of self-reactive B cells (Supplemental Fig. 4B). Additionally, after adoptively transferring Bm12 splenocytes, sera from BM chimeric mice with B cell–specific deletion of CARD19 showed significantly less autoreactive Abs when compared with control BM chimeric mice with wild-type B cells, as determined by both ANA ELISA and HEp-2 immunofluorescence assay (Supplemental Fig. 4C–E). The generation of GC B cells was also reduced in CARD19-deficient BM recipients compared with wild-type BM recipients after adoptively transferring Bm12 splenocytes (Supplemental Fig. 4F, 4G). These results demonstrate that CARD19 deficiency prevents autoimmunity in a B cell–intrinsic manner.

Discussion

Chronic stimulation of self-reactive B cells by self-antigens can weaken BCR signaling and ultimately lead to B cell tolerance. Negative regulators of BCR signaling, such as the tyrosine protein kinase Lyn, the protein phosphatase SHP-1, the lipid phosphatase SHIP-1, the inhibitory coreceptor CD22, and the ubiquitin ligases c-Cbl/Cbl-b, play an important role in controlling B cell tolerance (13–17). When a negative regulator of BCR-induced NF-κB pathway is deleted, it leads to B cell hyperactivation, elevation of autoantibody production, and subsequent severe autoimmune diseases (17, 57–59). In our study, we have identified the CARD-containing protein CARD19 as a novel negative regulatory molecule that controls TAK1 activity, downstream of the CBM signalosome, and regulates B cell tolerance through NF-κB–induced expression of Egr and Cbl in self-reactive B cells. In contrast to the deletion of traditional negative regulators of NF-κB signaling, deficiency in CARD19 does not result in autoimmune phenotypes. Instead, it enhances B cell tolerance, reduces autoantibody production, and prevents autoimmunity.

Upon BCR ligation, the scaffold protein CARMA1 (CARD11), together with BCL10 and MALT1, forms the CBM signalosome complex, which is central to the activation of the NF-κB signaling pathway (25, 70). The current studies found that CARD19 coimmunoprecipitated with TAK1, as well as CARMA1, TAB2, TRAF6, and NEMO, but not other components, such as BCL10, of the CBM signalosome or the downstream signaling cascade. However, the reciprocal co-IP analysis demonstrated that only TAK1 could associate with CARD19. These findings indicate that CARD19 directly interacts with TAK1, and its association with CARMA1, TAB2, TRAF6, and NEMO is likely to be indirect and due to the large signaling multiplex formed by the CBM signalosome, the TAK1 complex, and the IKK complex following BCR engagement. Activation of TAK1 requires its association with the regulatory proteins TAB1 and TAB2 (33–35). TAB1 and TAB2 are structurally different molecules with distinct roles in regulating TAK1 activity. TAB1 constitutively associates with the N terminus of TAK1 and regulates TAK1 autophosphorylation, which is required for TAK1 activation (33, 53). TAB2 interacts with the C terminus of TAK1 and induces TAK1 ubiquitination, which is required for its activation (34, 52). Furthermore, TAB2 binds to the polyubiquitin chain, recruiting polyubiquitinated TRAF6 and NEMO and bringing the IKK complex in close proximity to TAK1 (34, 52). Our findings indicate that CARD19 prevents TAK1 from interacting with TAB2 but not TAB1, and thus inhibits TAB2-mediated TAK1 ubiquitination. These data further support the idea that CARD19 directly interacts with TAK1 and that CARD19's co-IP with TAB2, TRAF6, and NEMO is due to the ubiquitination-dependent formation of the signaling multiplex comprising the TAK1 and IKK complexes. Therefore, CARD19 negatively regulates BCR-induced NF-κB activation by directly preventing the association of TAK1 with TAB2, thus impeding the ubiquitination and activation of TAK1.

NF-κB acts as a master regulator of the immune response, controlling the expression of various target genes that include cytokines, chemokines, immunoregulatory molecules, and molecules that direct cell proliferation and survival (71). When a negative regulator of the NF-κB pathway, such as c-Cbl, Cbl-b, PTPN22, Shp1, and A20, is deleted, it leads to hyperactive B cells, high autoantibody production, and severe autoimmunity (17, 57–59). In contrast, CARD19-deficient mice do not develop autoimmune phenotypes, although CARD19 negatively regulates the NF-κB pathway by inhibiting TAK1 activity. Instead, the lack of CARD19 enhances B cell tolerance, reduces autoantibody production, and prevents autoimmunity. This is likely because CARD19 deficiency only slightly elevates NF-κB signaling and this slight elevation does not affect BCR signaling in naive B cells and B cell development. Furthermore, foreign Ags, such as nitrophenyl–keyhole limpet hemocyanin or trinitrophenyl-Ficoll, normally initiate strong

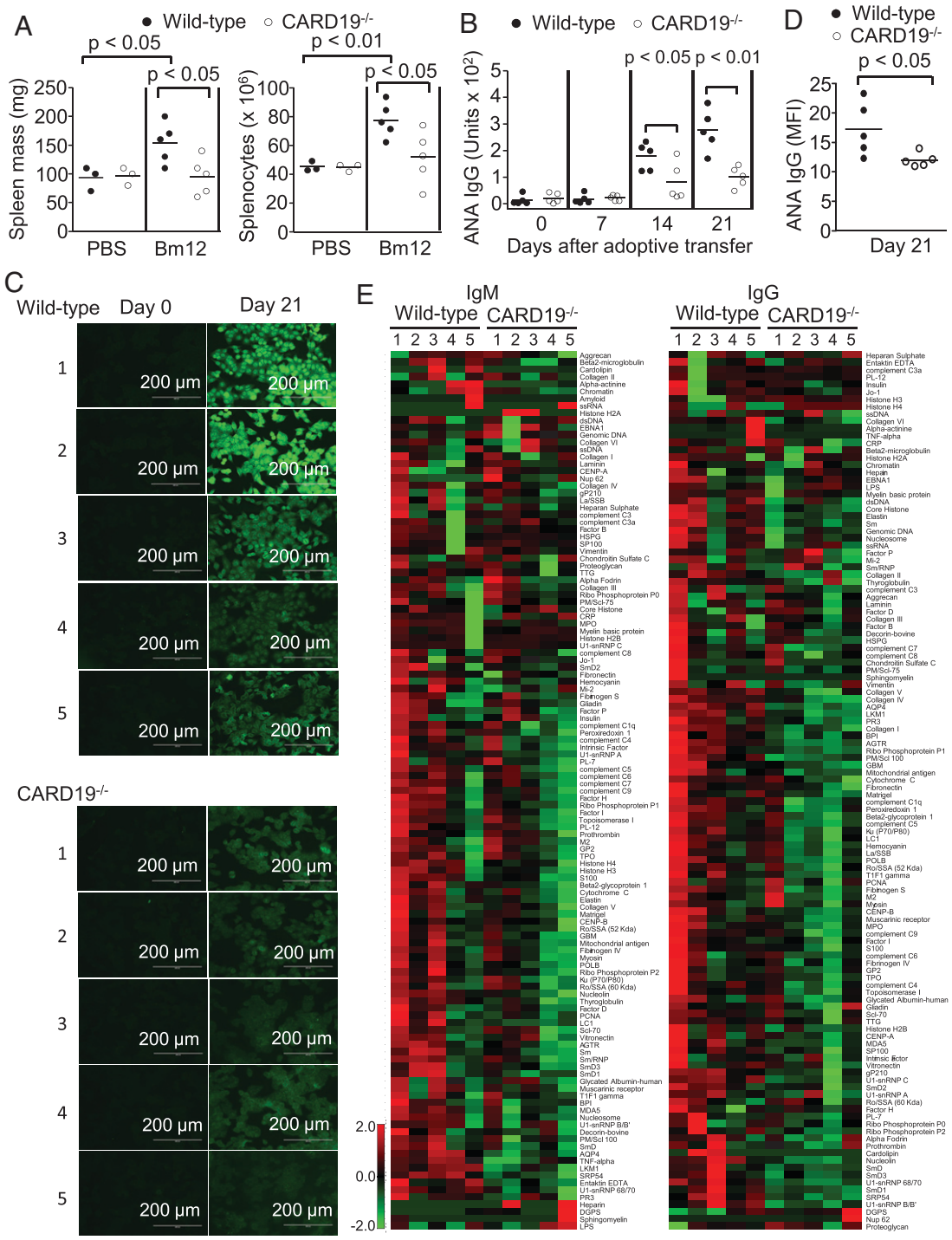

FIGURE 7. CARD19 deficiency prevents autoantibody production in the SLE mouse model. Splenocytes from Bm12 mice or PBS were adoptively transferred into age- and sex-matched CD45.1 congenic recipients that were reconstituted with wild-type or CARD19$^{-/-}$ BM cells. (**A**) Inhibition of Bm12-induced splenomegaly by CARD19 deficiency. Spleen mass and cell number of spleen cells in the recipients were determined at day 21 after adoptive transfer. (**B**) Inhibition of Bm12-induced production of ANA IgG by CARD19 deficiency. Sera from the recipients were collected at the indicated time points after adoptive transfer. ANA IgG levels were measured by the ANA IgG ELISA. (**C** and **D**) Inhibition of Bm12-induced production of autoreactive IgGs reactive to HEp-2 cells by CARD19 deficiency. Sera from the recipients were collected at day 21 after adoptive transfer and incubated with HEp-2 cells. Serum ANA IgGs were detected by immunofluorescence on HEp-2 cells (C) and immunofluorescence intensities were quantified using ImageJ software (D). (**E**) Inhibition of Bm12-induced autoantibody production by CARD19 deficiency. Sera from the recipients were collected at day 21 after adoptive transfer and subjected to a self-antigen array for detecting self-reactive IgM and IgG. Each column represents an individual mouse and each row represents an individual self-antigen. Red, green, and black grid blocks indicate expression above, below, and at the median of all samples at each row. Each dot represents an individual mouse and horizontal lines represent the mean values. The *p* values shown were calculated with an unpaired two-tailed Student *t* test. Data shown were obtained from five recipients that received wild-type or CARD19$^{-/-}$ BM cells and are representative of two independent experiments.

and robust BCR signaling that can overcome the slight elevation of NF-κB signaling caused by CARD19 deficiency. Consistent with this idea, CARD19 deficiency does not affect the humoral immune response. However, we believe that constant engagement of BCR by weak self-antigens induces moderate but persistent signaling in self-reactive B cells. In the absence of CARD19, moderate but

persistent BCR signaling combined with the subtle elevation of NF-κB activation leads to the accumulation of the negative regulators Egr and Cbl, which in turn promotes tolerance in self-reactive B cells (a proposed working model is shown in the visual abstract that appears in the online version of this article). In contrast to the conventional negative regulators of NF-κB activation, CARD19 exhibits a unique and distinct role in modulating BCR-induced NF-κB activation in self-reactive B cells and its deficiency enhances but does not break B cell tolerance.

The molecular mechanism that underlies the expression of the E3 ubiquitin ligase Cbl in B cells is not well understood. Studies have shown that ionomycin stimulation induces Cbl expression in T cells (65), indicating the involvement of Ca^{2+}-mediated activation of the transcription factor NFAT in Cbl expression in T cells. However, our findings indicate that the PKC activator PDBu, but not ionomycin, is able to trigger Cbl expression in B cells, suggesting that PKC-induced NF-κB activation could control Cbl expression in B cells. Furthermore, Cbl expression is substantially reduced in B cells that lack c-Rel, a key member of NF-κB. These results reveal that the expression of Cbl, such as c-Cbl and Cbl-b, is regulated by NF-κB and not NFAT in B cells, highlighting the differential regulation of Cbl expression in B and T cells.

Egrs are zinc-finger transcription factors that are upregulated in response to growth factors (72). Among the four Egr isoforms, Egr2 and Egr3 are particularly important for establishing T and B cell anergy and tolerance (63, 73–75). Deletion of both Egr2 and Egr3 in T cells leads to high production of antinuclear autoantibodies, proinflammatory cytokines, and the development of SLE-like autoimmune syndrome (74). In T cells, overexpression of Egr2 and Egr3 can upregulate the expression of Cbl-b, whereas the loss of Egr3 markedly reduces Cbl-b expression (63). These findings demonstrate that Cbl-b is a downstream target of Egr2 and Egr3 in T cells. Our research has found that CARD19 deficiency elevates the basal and BCR-induced expression of Egr2 and Egr3 in B cells. It is highly likely that the upregulation of Egr2 and Egr3 leads to an elevation of c-Cbl and Cbl-b expression in B cells, which results in enhanced tolerance of self-reactive B cells (see the visual abstract that appears in the online version of this article). In T cells, both Egr2 and Egr3 are NFAT target genes (66). However, we found that the PKC activator PDBu, but not the Ca^{2+} inducer ionomycin, was able to trigger the expression of Egr2 and Egr3. Furthermore, c-Rel–deficient B cells exhibited marked reduction of Egr2 and Egr3 expression, confirming that the expression of Erg2 and Egr3 is dependent on NF-κB but not NFAT in B cells. Taken together, these results demonstrate that in self-reactive B cells, CARD19 deficiency augments BCR-induced TAK1 activity, which leads to an elevation of NF-κB activation that triggers Egr2 and Egr3 expression, ultimately inducing the accumulation of c-Cbl and Cbl-b. While in T cells Egr2/3 and Cbls are regulated by NFAT, in B cells they are regulated by NF-κB. However, the molecular mechanism underlying the differential regulation of Egr2/3 and Cbl expression in B and T cells is not well understood and requires further investigation.

In summary, the study has found that CARD19 plays an important role in regulating TAK1 activity and B cell tolerance. Specifically, it has been shown that CARD19 interacts with TAK1, preventing its association with TAB2 and limiting its ubiquitination and activation. CARD19 deficiency results in a subtle elevation of NF-κB activation in self-reactive B cells, which leads to the accumulation of the negative regulators Egr and Cbl. This in turn enhances B cell tolerance and reduces autoantibody production, preventing autoimmune diseases. Taken together, these findings suggest that targeting CARD19 in B cells could be a potential therapeutic strategy for treating autoimmune diseases.

Acknowledgments

We acknowledge Robert Burns and Shikan Zheng for assistance with analysis of the high-throughput sequencing data.

Disclosures

The authors have no financial conflicts of interest.

References

1. Healy, J. I., and C. C. Goodnow. 1998. Positive versus negative signaling by lymphocyte antigen receptors. *Annu. Rev. Immunol.* 16: 645–670.
2. Hardy, R. R., and K. Hayakawa. 2001. B cell development pathways. *Annu. Rev. Immunol.* 19: 595–621.
3. Loder, F., B. Mutschler, R. J. Ray, C. J. Paige, P. Sideras, R. Torres, M. C. Lamers, and R. Carsetti. 1999. B cell development in the spleen takes place in discrete steps and is determined by the quality of B cell receptor-derived signals. *J. Exp. Med.* 190: 75–89.
4. Nemazee, D. A., and K. Bürki. 1989. Clonal deletion of B lymphocytes in a transgenic mouse bearing anti-MHC class I antibody genes. *Nature* 337: 562–566.
5. Hartley, S. B., J. Crosbie, R. Brink, A. B. Kantor, A. Basten, and C. C. Goodnow. 1991. Elimination from peripheral lymphoid tissues of self-reactive B lymphocytes recognizing membrane-bound antigens. *Nature* 353: 765–769.
6. Gay, D., T. Saunders, S. Camper, and M. Weigert. 1993. Receptor editing: an approach by autoreactive B cells to escape tolerance. *J. Exp. Med.* 177: 999–1008.
7. Tiegs, S. L., D. M. Russell, and D. Nemazee. 1993. Receptor editing in self-reactive bone marrow B cells. *J. Exp. Med.* 177: 1009–1020.
8. Goodnow, C. C., J. Crosbie, S. Adelstein, T. B. Lavoie, S. J. Smith-Gill, R. A. Brink, H. Pritchard-Briscoe, J. S. Wotherspoon, R. H. Loblay, K. Raphael, et al. 1988. Altered immunoglobulin expression and functional silencing of self-reactive B lymphocytes in transgenic mice. *Nature* 334: 676–682.
9. Eris, J. M., A. Basten, R. Brink, K. Doherty, M. R. Kehry, and P. D. Hodgkin. 1994. Anergic self-reactive B cells present self antigen and respond normally to CD40-dependent T-cell signals but are defective in antigen-receptor-mediated functions. *Proc. Natl. Acad. Sci. USA* 91: 4392–4396.
10. Merrell, K. T., R. J. Benschop, S. B. Gauld, K. Aviszus, D. Decote-Ricardo, L. J. Wysocki, and J. C. Cambier. 2006. Identification of anergic B cells within a wild-type repertoire. *Immunity* 25: 953–962.
11. Gauld, S. B., R. J. Benschop, K. T. Merrell, and J. C. Cambier. 2005. Maintenance of B cell anergy requires constant antigen receptor occupancy and signaling. *Nat. Immunol.* 6: 1160–1167.
12. Healy, J. I., R. E. Dolmetsch, L. A. Timmerman, J. G. Cyster, M. L. Thomas, G. R. Crabtree, R. S. Lewis, and C. C. Goodnow. 1997. Different nuclear signals are activated by the B cell receptor during positive versus negative signaling. *Immunity* 6: 419–428.
13. Hibbs, M. L., D. M. Tarlinton, J. Armes, D. Grail, G. Hodgson, R. Maglitto, S. A. Stacker, and A. R. Dunn. 1995. Multiple defects in the immune system of Lyn-deficient mice, culminating in autoimmune disease. *Cell* 83: 301–311.
14. Cyster, J. G., and C. C. Goodnow. 1995. Protein tyrosine phosphatase 1C negatively regulates antigen receptor signaling in B lymphocytes and determines thresholds for negative selection. *Immunity* 2: 13–24.
15. O'Keefe, T. L., G. T. Williams, S. L. Davies, and M. S. Neuberger. 1996. Hyperresponsive B cells in CD22-deficient mice. *Science* 274: 798–801.
16. O'Neill, S. K., A. Getahun, S. B. Gauld, K. T. Merrell, I. Tamir, M. J. Smith, J. M. Dal Porto, Q. Z. Li, and J. C. Cambier. 2011. Monophosphorylation of CD79a and CD79b ITAM motifs initiates a SHIP-1 phosphatase-mediated inhibitory signaling cascade required for B cell anergy. *Immunity* 35: 746–756.
17. Kitaura, Y., I. K. Jang, Y. Wang, Y. C. Han, T. Inazu, E. J. Cadera, M. Schlissel, R. R. Hardy, and H. Gu. 2007. Control of the B cell-intrinsic tolerance programs by ubiquitin ligases Cbl and Cbl-b. *Immunity* 26: 567–578.
18. Karasuyama, H., A. Kudo, and F. Melchers. 1990. The proteins encoded by the VpreB and lambda 5 pre-B cell-specific genes can associate with each other and with mu heavy chain. *J. Exp. Med.* 172: 969–972.
19. Tsubata, T., and M. Reth. 1990. The products of pre-B cell-specific genes (lambda 5 and VpreB) and the immunoglobulin mu chain form a complex that is transported onto the cell surface. *J. Exp. Med.* 172: 973–976.
20. Hombach, J., T. Tsubata, L. Leclercq, H. Stappert, and M. Reth. 1990. Molecular components of the B-cell antigen receptor complex of the IgM class. *Nature* 343: 760–762.
21. Harwood, N. E., and F. D. Batista. 2010. Early events in B cell activation. *Annu. Rev. Immunol.* 28: 185–210.
22. Kaileh, M., and R. Sen. 2012. NF-κB function in B lymphocytes. *Immunol. Rev.* 246: 254–271.
23. Gerondakis, S., and U. Siebenlist. 2010. Roles of the NF-κB pathway in lymphocyte development and function. *Cold Spring Harb. Perspect. Biol.* 2: a000182.
24. Miraghazadeh, B., and M. C. Cook. 2018. Nuclear factor-kappaB in autoimmunity: man and mouse. *Front. Immunol.* 9: 613.
25. Lin, X., and D. Wang. 2004. The roles of CARMA1, Bcl10, and MALT1 in antigen receptor signaling. *Semin. Immunol.* 16: 429–435.
26. Thome, M. 2004. CARMA1, BCL-10 and MALT1 in lymphocyte development and activation. *Nat. Rev. Immunol.* 4: 348–359.
27. Egawa, T., B. Albrecht, B. Favier, M.-J. Sunshine, K. Mirchandani, W. O'Brien, M. Thome, and D. R. Littman. 2003. Requirement for CARMA1 in antigen

receptor-induced NF-κB activation and lymphocyte proliferation. *Curr. Biol.* 13: 1252–1258.
28. Hara, H., T. Wada, C. Bakal, I. Kozieradzki, S. Suzuki, N. Suzuki, M. Nghiem, E. K. Griffiths, C. Krawczyk, B. Bauer, et al. 2003. The MAGUK family protein CARD11 is essential for lymphocyte activation. *Immunity* 18: 763–775.
29. Xue, L., S. W. Morris, C. Orihuela, E. Tuomanen, X. Cui, R. Wen, and D. Wang. 2003. Defective development and function of Bcl10-deficient follicular, marginal zone and B1 B cells. *Nat. Immunol.* 4: 857–865.
30. Ruefli-Brasse, A. A., D. M. French, and V. M. Dixit. 2003. Regulation of NF-κB-dependent lymphocyte activation and development by paracaspase. *Science* 302: 1581–1584.
31. Ruland, J., G. S. Duncan, A. Wakeham, and T. W. Mak. 2003. Differential requirement for Malt1 in T and B cell antigen receptor signaling. *Immunity* 19: 749–758.
32. Schuman, J., Y. Chen, A. Podd, M. Yu, H. H. Liu, R. Wen, Z. J. Chen, and D. Wang. 2009. A critical role of TAK1 in B-cell receptor-mediated nuclear factor κB activation. *Blood* 113: 4566–4574.
33. Shibuya, H., K. Yamaguchi, K. Shirakabe, A. Tonegawa, Y. Gotoh, N. Ueno, K. Irie, E. Nishida, and K. Matsumoto. 1996. TAB1: an activator of the TAK1 MAPKKK in TGF-β signal transduction. *Science* 272: 1179–1182.
34. Wang, C., L. Deng, M. Hong, G. R. Akkaraju, J. Inoue, and Z. J. Chen. 2001. TAK1 is a ubiquitin-dependent kinase of MKK and IKK. *Nature* 412: 346–351.
35. Takaesu, G., S. Kishida, A. Hiyama, K. Yamaguchi, H. Shibuya, K. Irie, J. Ninomiya-Tsuji, and K. Matsumoto. 2000. TAB2, a novel adaptor protein, mediates activation of TAK1 MAPKKK by linking TAK1 to TRAF6 in the IL-1 signal transduction pathway. *Mol. Cell* 5: 649–658.
36. Sun, L., L. Deng, C. K. Ea, Z. P. Xia, and Z. J. Chen. 2004. The TRAF6 ubiquitin ligase and TAK1 kinase mediate IKK activation by BCL10 and MALT1 in T lymphocytes. *Mol. Cell* 14: 289–301.
37. Karin, M., and Y. Ben-Neriah. 2000. Phosphorylation meets ubiquitination: the control of NF-κB activity. *Annu. Rev. Immunol.* 18: 621–663.
38. Ghosh, S., M. J. May, and E. B. Kopp. 1998. NF-κB and Rel proteins: evolutionarily conserved mediators of immune responses. *Annu. Rev. Immunol.* 16: 225–260.
39. Park, H. H. 2019. Caspase recruitment domains for protein interactions in cellular signaling (Review). *Int. J. Mol. Med.* 43: 1119–1127.
40. Woo, H.-N., G.-S. Hong, J.-I. Jun, D.-H. Cho, H. W. Choi, H.-J. Lee, C.-W. Chung, I.-K. Kim, D.-G. Jo, J.-O. Pyo, et al. 2004. Inhibition of Bcl10-mediated activation of NF-κB by BinCARD, a Bcl10-interacting CARD protein. *FEBS Lett.* 578: 239–244.
41. Rios, K. E., A. K. Kashyap, S. K. Maynard, M. Washington, S. Paul, and B. C. Schaefer. 2020. CARD19, the protein formerly known as BinCARD, is a mitochondrial protein that does not regulate Bcl10-dependent NF-κB activation after TCR engagement. *Cell. Immunol.* 356: 104179.
42. Suzuki, H., T. Kameyama, and A. Takaoka. 2019. BinCARD2 as a positive regulator of interferon response in innate immunity. *Biochem. Biophys. Res. Commun.* 511: 287–293.
43. Wang, D., J. Feng, R. Wen, J. C. Marine, M. Y. Sangster, E. Parganas, A. Hoffmeyer, C. W. Jackson, J. L. Cleveland, P. J. Murray, and J. N. Ihle. 2000. Phospholipase Cγ2 is essential in the functions of B cell and several Fc receptors. *Immunity* 13: 25–35.
44. Dai, X., Y. Chen, L. Di, A. Podd, G. Li, K. D. Bunting, L. Hennighausen, R. Wen, and D. Wang. 2007. Stat5 is essential for early B cell development but not for B cell maturation and function. *J. Immunol.* 179: 1068–1079.
45. Kuraoka, M., A. G. Schmidt, T. Nojima, F. Feng, A. Watanabe, D. Kitamura, S. C. Harrison, T. B. Kepler, and G. Kelsoe. 2016. Complex antigens drive permissive clonal selection in germinal centers. *Immunity* 44: 542–552.
46. Love, M. I., W. Huber, and S. Anders. 2014. Moderated estimation of fold change and dispersion for RNA-seq data with DESeq2. *Genome Biol.* 15: 550.
47. Ritchie, M. E., B. Phipson, D. Wu, Y. Hu, C. W. Law, W. Shi, and G. K. Smyth. 2015. limma powers differential expression analyses for RNA-sequencing and microarray studies. *Nucleic Acids Res.* 43: e47.
48. Yu, G., L. G. Wang, Y. Han, and Q. Y. He. 2012. clusterProfiler: an R package for comparing biological themes among gene clusters. *OMICS* 16: 284–287.
49. Kanehisa, M., and S. Goto. 2000. KEGG: Kyoto Encyclopedia of Genes and Genomes. *Nucleic Acids Res.* 28: 27–30.
50. Fabregat, A., S. Jupe, L. Matthews, K. Sidiropoulos, M. Gillespie, P. Garapati, R. Haw, B. Jassal, F. Korninger, B. May, et al. 2018. The Reactome Pathway Knowledgebase. *Nucleic Acids Res.* 46(D1): D649–D655.
51. Benjamini, Y., and Y. Hochberg. 1995. Controlling the false discovery rate: a practical and powerful approach to multiple testing. *J. R. Stat. Soc. B* 57: 289–300.
52. Kanayama, A., R. B. Seth, L. Sun, C. K. Ea, M. Hong, A. Shaito, Y. H. Chiu, L. Deng, and Z. J. Chen. 2004. TAB2 and TAB3 activate the NF-κB pathway through binding to polyubiquitin chains. *Mol. Cell* 15: 535–548.
53. Kishimoto, K., K. Matsumoto, and J. Ninomiya-Tsuji. 2000. TAK1 mitogen-activated protein kinase kinase kinase is activated by autophosphorylation within its activation loop. *J. Biol. Chem.* 275: 7359–7364.
54. Wan, Y. Y., H. Chi, M. Xie, M. D. Schneider, and R. A. Flavell. 2006. The kinase TAK1 integrates antigen and cytokine receptor signaling for T cell development, survival and function. *Nat. Immunol.* 7: 851–858.
55. Liu, H. H., M. Xie, M. D. Schneider, and Z. J. Chen. 2006. Essential role of TAK1 in thymocyte development and activation. *Proc. Natl. Acad. Sci. USA* 103: 11677–11682.
56. Sato, S., H. Sanjo, K. Takeda, J. Ninomiya-Tsuji, M. Yamamoto, T. Kawai, K. Matsumoto, O. Takeuchi, and S. Akira. 2005. Essential function for the kinase TAK1 in innate and adaptive immune responses. *Nat. Immunol.* 6: 1087–1095.
57. Pao, L. I., K. P. Lam, J. M. Henderson, J. L. Kutok, M. Alimzhanov, L. Nitschke, M. L. Thomas, B. G. Neel, and K. Rajewsky. 2007. B cell-specific deletion of protein-tyrosine phosphatase Shp1 promotes B-1a cell development and causes systemic autoimmunity. *Immunity* 27: 35–48.
58. Dai, X., R. G. James, T. Habib, S. Singh, S. Jackson, S. Khim, R. T. Moon, D. Liggitt, A. Wolf-Yadlin, J. H. Buckner, and D. J. Rawlings. 2013. A disease-associated *PTPN22* variant promotes systemic autoimmunity in murine models. *J. Clin. Invest.* 123: 2024–2036.
59. Tavares, R. M., E. E. Turer, C. L. Liu, R. Advincula, P. Scapini, L. Rhee, J. Barrera, C. A. Lowell, P. J. Utz, B. A. Malynn, and A. Ma. 2010. The ubiquitin modifying enzyme A20 restricts B cell survival and prevents autoimmunity. *Immunity* 33: 181–191.
60. Cambier, J. C., S. B. Gauld, K. T. Merrell, and B. J. Vilen. 2007. B-cell anergy: from transgenic models to naturally occurring anergic B cells? *Nat. Rev. Immunol.* 7: 633–643.
61. Suvas, S., V. Singh, S. Sahdev, H. Vohra, and J. N. Agrewala. 2002. Distinct role of CD80 and CD86 in the regulation of the activation of B cell and B cell lymphoma. *J. Biol. Chem.* 277: 7766–7775.
62. Mecklenbräuker, I., K. Saijo, N. Y. Zheng, M. Leitges, and A. Tarakhovsky. 2002. Protein kinase Cδ controls self-antigen-induced B-cell tolerance. *Nature* 416: 860–865.
63. Safford, M., S. Collins, M. A. Lutz, A. Allen, C. T. Huang, J. Kowalski, A. Blackford, M. R. Horton, C. Drake, R. H. Schwartz, and J. D. Powell. 2005. Egr-2 and Egr-3 are negative regulators of T cell activation. [Published erratum appears in 2005 *Nat. Immunol.* 6: 737.] *Nat. Immunol.* 6: 472–480 .
64. Yu, M., Y. Chen, H. Zeng, Y. Zheng, G. Fu, W. Zhu, U. Broeckel, P. Aggarwal, A. Turner, G. Neale, et al. 2017. PLCγ-dependent mTOR signalling controls IL-7-mediated early B cell development. *Nat. Commun.* 8: 1457.
65. Jeon, M. S., A. Atfield, K. Venuprasad, C. Krawczyk, R. Sarao, C. Elly, C. Yang, S. Arya, K. Bachmaier, L. Su, et al. 2004. Essential role of the E3 ubiquitin ligase Cbl-b in T cell anergy induction. *Immunity* 21: 167–177.
66. Rengarajan, J., P. R. Mittelstadt, H. W. Mages, A. J. Gerth, R. A. Kroczek, J. D. Ashwell, and L. H. Glimcher. 2000. Sequential involvement of NFAT and Egr transcription factors in FasL regulation. *Immunity* 12: 293–300.
67. Grumont, R. J., I. J. Rourke, L. A. O'Reilly, A. Strasser, K. Miyake, W. Sha, and S. Gerondakis. 1998. B lymphocytes differentially use the Rel and nuclear factor κB1 (NF-κB1) transcription factors to regulate cell cycle progression and apoptosis in quiescent and mitogen-activated cells. *J. Exp. Med.* 187: 663–674.
68. Dörner, T., and R. Furie. 2019. Novel paradigms in systemic lupus erythematosus. *Lancet* 393: 2344–2358.
69. Morris, S. C., P. L. Cohen, and R. A. Eisenberg. 1990. Experimental induction of systemic lupus erythematosus by recognition of foreign Ia. *Clin. Immunol. Immunopathol.* 57: 263–273.
70. Rawlings, D. J., K. Sommer, and M. E. Moreno-García. 2006. The CARMA1 signalosome links the signalling machinery of adaptive and innate immunity in lymphocytes. *Nat. Rev. Immunol.* 6: 799–812.
71. Oeckinghaus, A., and S. Ghosh. 2009. The NF-κB family of transcription factors and its regulation. *Cold Spring Harb. Perspect. Biol.* 1: a000034.
72. O'Donovan, K. J., W. G. Tourtellotte, J. Millbrandt, and J. M. Baraban. 1999. The EGR family of transcription-regulatory factors: progress at the interface of molecular and systems neuroscience. *Trends Neurosci.* 22: 167–173.
73. Zhu, B., A. L. Symonds, J. E. Martin, D. Kioussis, D. C. Wraith, S. Li, and P. Wang. 2008. Early growth response gene 2 (Egr-2) controls the self-tolerance of T cells and prevents the development of lupuslike autoimmune disease. *J. Exp. Med.* 205: 2295–2307.
74. Li, S., T. Miao, M. Sebastian, P. Bhullar, E. Ghaffari, M. Liu, A. L. Symonds, and P. Wang. 2012. The transcription factors Egr2 and Egr3 are essential for the control of inflammation and antigen-induced proliferation of B and T cells. *Immunity* 37: 685–696.
75. Zheng, Y., Y. Zha, G. Driessens, F. Locke, and T. F. Gajewski. 2012. Transcriptional regulator early growth response gene 2 (Egr2) is required for T cell anergy in vitro and in vivo. *J. Exp. Med.* 209: 2157–2163.